

Printing a Glass Ecology

by

Daniel Lizardo

B.S. Materials Science and Engineering, Massachusetts Institute of
Technology (2015)

Submitted to the Program in Media Arts and Sciences
in partial fulfillment of the requirements for the degree of

Masters of Science in Media Arts and Sciences

at the

MASSACHUSETTS INSTITUTE OF TECHNOLOGY

June 2018

© Massachusetts Institute of Technology 2018. All rights reserved.

 Signature redacted

Author

 Program in Media Arts and Sciences
May 11, 2018

 Signature redacted

Certified by

 Meri Oxman
Associate Professor
Thesis Supervisor

 Signature redacted

Accepted by

 Tod Machover
Associate Academic Head, Program in Media Arts and Sciences

Printing a Glass Ecology

by

Daniel Lizardo

Submitted to the Program in Media Arts and Sciences
in partial fulfillment of the requirements for the degree of

Masters of Science in Media Arts and Sciences

at the

MASSACHUSETTS INSTITUTE OF TECHNOLOGY

June 2018

© Massachusetts Institute of Technology 2018. All rights reserved.

Signature redacted

Approved by.....

.....
Peter Houk
Director, MIT Glass Lab

Printing a Glass Ecology

by

Daniel Lizardo

Submitted to the Program in Media Arts and Sciences
in partial fulfillment of the requirements for the degree of

Masters of Science in Media Arts and Sciences

at the

MASSACHUSETTS INSTITUTE OF TECHNOLOGY

June 2018

© Massachusetts Institute of Technology 2018. All rights reserved.

Signature redacted

Approved by.....

Assistant Professor of Design Research, Department of Architecture

 Skylar Tibbits

Acknowledgments

This work is dedicated the team who has enabled it, driven it, and strive to make their visions a reality, to challenge what has been known, and produce something amazing. They live this effort every day, from the first prototype, to an unknown and unbounded future.

Thank you Chikara Inamura, Michael Stern, Peter Houk, and Neri Oxman.

I am immensely proud of what we have accomplished, this team pushing me to learn and grow, and with them, the greater family of The Mediated Matter Group supports and cultivates a culture of challenging science, thoughtful design, and support of each other.

Thank you Jorge Duro-Royo, Laia Mogas-Soldevilla, John Klein, Markus Kayser, Steven Keating, William Patrick, Sunanda Sharma, Julian Leland, Christoph Bader, Dominik Kolb, Rachel Smith, Tim Tai, Andrea Ling, Levi Cai, João Costa, Sara Falcone, Josh Van Zak, Zijay Tang, Barrak Darweesh, Jean Disset, James Weaver, Kelly Donovan, Andrea Porras, Natalia Casas, Tal Aчитув, Tomer Weller, Owen Trueblood, Nassia Inglessis, Giorgia Franchin.

Abstract

In this thesis, I explore relationships between form generation, material properties, and design constraints in search of a new framework for designing with unpredictable or unstable material systems using glass 3D printing as a case study. Molten glass forming has always been difficult to accurately predict or model, but also offers a high degree of geometric complexity or hierarchy through organic formations.

Top-down design approaches to material tunability and control are enabled by new digital fabrication tools and technologies that offer some of most successful attempts to design at scales approaching that of nature [38] [20]. Bottom-up, material-driven systems design functionality, itself, around organically formed structures to challenge our perspective of designing for utility, and how to define that utility [18]. The glass 3D printer, developed by The Mediated Matter Group in collaboration with the MIT Glass Lab, has been an important case study long in the making. A novel type of glass forming quickly gave way to a dialogue with highly unstable material behaviors, structures too complex to model in real time and visually compelling, frozen in time with cooling temperatures. The process generates new types of glass structures and visual output, enabling new design typologies for the product and architectural scale.

Here I present an array of over a hundred unique design experiments that offer insight into this brand new design space created by complex glass behavior under control of a digital machine and harnessing structural instability. Close study not only of the objects generated but also their behavior during fabrication is key to understanding how the glass responds to the motion of the machine. Analysis of the project workflow itself provides the foundation for a framework capable of handling an active and complex material system, identifying how and when machine control can be used directly, how and when organic material formation can take place, and how the two interface from design tool to fabrication tool to design product.

Finally, I look ahead to the potential for new product and architectural functionalities enabled by this platform, and I establish concepts for using the highly complex forms with the mapped "design space" as a guide for what we understand to be possible. The goal is to form new knowledge about material-informed digital fabrication through the generation of new glass forms and designs.

Contents

1	Introduction	8
1.1	New Evolution of Fabrication Technology	8
1.1.1	Fabrication Information Modeling - Mediated Matter	9
1.1.2	Post-Digital Design	12
1.1.3	Emergent Design of Products	13
2	Motivation: Glass Fabrication from Hand Tools to Industrial Additive Manufacturing	17
2.1	Glass and the Built Environment	18
2.2	Glass in Architecture	18
2.3	Printed Glass	19
2.3.1	Goals for Glass 3D Printer G3DP2	20
2.4	New Platform - From Prototype to Industrial Platform	21
2.4.1	System Architecture	21
2.4.2	Platform Operation	22
2.5	Towards New Glass Products	23
3	Design Space	24
3.1	G3DP and G3DP2	24
3.1.1	G3DP: The First Stages of Material Information and Novel Design Methods	24
3.1.2	Lessons From G3DP and Exhibition	26
3.1.3	G3DP2: platform redesign and description	30
3.1.4	Public Installation of Glass Structure, Milan Design Week 2017	32
3.2	Forward Development	34
3.2.1	Tracking the System	37
3.2.2	Future Machine Information and Tools	44
3.2.3	Feed Rate and Layer Height	46

3.2.4	Curvature, Draft Angle, and Free Path Printing . . .	50
3.2.5	Conclusion of Forward Development	58
3.3	Sub-filament Scale Fabrication	59
3.3.1	Autocoiling Phenomenon	59
3.3.2	Bridging	62
3.3.3	Towards a New Product Space	64
4	Conclusion: Towards Vascular Architecture	65
4.1	3D Printed Vessels	65
4.1.1	Bilobe Design and First Principles of Multi-Channel Glass	67
4.1.2	Active Z Toolpathing	70
4.1.3	Further Experiments and Potential Applications . . .	71
4.2	Vascular Architecture in the Future	76
4.2.1	Preliminary Environmental Models	76
4.2.2	Preliminary Performance Testing	80
4.3	Conclusion	85
	References	86

Chapter 1

Introduction

1.1 New Evolution of Fabrication Technology

designing by, with, and for nature

MIT's Professor Neri Oxman [26] describes a reorganized design philosophy where design is a practice of connectivity between fabrication, product, and environment. We understand that the most complex natural systems are driven by hierarchies of thermodynamic interactions, which function with the aim only to minimize energy. It is the networking of those functions, which produces structures, life, and even intelligence. The natural world designs implicitly, rather than explicitly, and designers have been able to leverage this philosophy through the use of highly sophisticated computational design tools. From the broadest ideas of parametric design, defining optimized geometry through the use of parametric equations, through generative design, and to "biomimetic" design tools that borrow directly from natural systems for use in form-finding, the computational design world has been able to model and define form at scales which truly approach that of the natural world [28]. But while geometric modeling and representation continues to advance in fidelity and scale, its translation to the physical world remains a serious challenge. There are similarities between modeling for representation and modeling for physical accountability. The closer a digital physics engine can get to real world mechanics, the more real it appears to the viewer – to the point of even a post-truth graphical world [41] – but perceived realism is not the same as fabrication accountability, especially when materials systems behave in a non-deterministic manner. And the higher the design resolution,

the more fabrication tools must work to remain accountable. The vision of this thesis is to look towards a new type of understanding of the behavior of the natural world, the materials in it and tools we use to operate on them, in order to more efficiently use materials as well as find new utility in ones which are too unstable to fit traditional fabrication methods.

I am beginning with examples of fabrication technologies that are material-sensitive at a core level (Fabrication Information Technology, Jorge Duro, MIT Media Lab), post-digital in design philosophy (Plato's Columns, Sandra Manninger and Matias Del Campo, University of Michigan), and emergent in fabrication output (Emerging Objects, University of California Berkley). These experimental design research efforts set a diverse context in which the glass 3D printing process was developed. It contains aspects of each philosophy, highlighting the flexibility of the project in terms of research vector, but also the flexibility how a design space may be perceived. Researchers view the same design problem through different lenses, seeing it as a *challenge* of material sensitivity, an *opportunity* of post-digital aesthetic, or the *utility* of emergent properties. Each view brings different analysis to the fabrication results, and through experimenting in glass printing, the process proved to show novel results to many different ends.

1.1.1 Fabrication Information Modeling - Mediated Matter

A new philosophy in design workflow under development in the Mediated Matter group seeks to bridge the gap between high spatial resolution computer aided design (CAD) and high spatial accuracy digital or computer numerically controlled (CNC) fabrication technology. Digital modeling can be accomplished at as high a resolution as is affordable to increasingly powerful computational hardware. Intelligent programming of CAD software is built not on discrete geometry but constructions of continuous mathematical functions which define curves and surfaces in 3D space. Rather than store discrete 3D data, which scales with the size of the design, continuous functions can define geometry at any scale. A rendering framework can evaluate functions at any spatial resolution or viewing window to provide an 'infinitely' accurate design, a powerful utility in being able to design at many scales without prohibitively large digital files.

The utility gap appears when we consider that, of course, physical materials and their fabrication can never be as accurately defined. There will always be a tolerance in how a design is exported, a tolerance in how hands and machines match that exported resolution, and finally a tolerance in the phys-

ical material itself. Tolerances at normal scales can be accurately calculated and accounted for in modern design and construction. Building Information Modeling (BIM) describes a workflow in which designs are generated and rendered at computer resolution but carry the auxiliary information about their fabrication tolerance with them. The most complex construction systems use BIM to successfully carry parametric designs into fabrication from product to architectural and urban scale by pairing designs with information about how they are fabricated and how they will fit together in the physical world [19]. Looking ahead to the future of design, we understand and create functionalities at increasingly disparate scales, leveraging micro- and nano-scale fabrication to product scale functionalities such as structural color [45] and physical dynamics [21]. As designs reach across more scales, the efficacy of BIM systems is pushed to its limits when functionality approach scales of modern fabrication tolerances. In order to rethink the design workflow from the ground up, researchers in The Mediated Matter group take a fabrication-sensitive approach to design, a philosophy termed *Fabrication Informed Modeling* (FIM) [22]. The term describes a process in which information about material and fabrication process are integral to the modeling of form. Unlike with BIM systems however, that information is not auxiliary, but shares dimensionality with the design itself, constraining the designer to forms that can actually be fabricated. The concept is not completely novel; for example, a software for designing parts to be CNC abrasive waterjet cut (Omax Layout, OMAX Corporation) generates part drawings with kerf ¹ included in all 2D and 3D geometries, explicitly accounting for that specific machine physics and enabling high precision parts. The result is extreme levels of geometric accuracy (within $1/10000in$), but also a highly specific standalone software platform. The FIM approach applies such material and fabrication sensitivity not just post-design but integrated in the design process. Rather than applying constraints to geometry which is already penned, it seeks to offer a holistic approach to designing both within constraints, and also designing in such a way that takes advantage of material interactions in the fabrication process. A forerunning case study in this methodology is the additive manufacturing (AM) of biologically generated hydrogels at large scales [25].

¹the groove or slit created by the width of the cutting tool or process

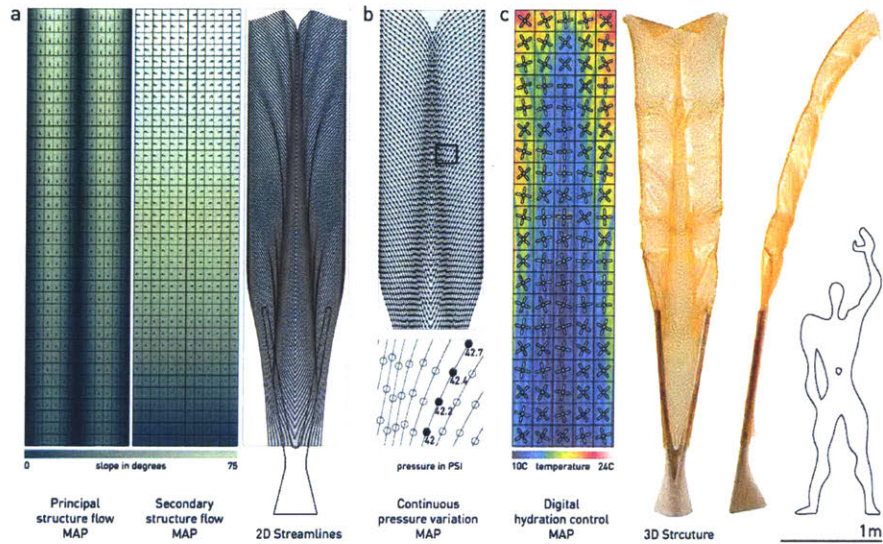


Figure 1-1: design workflow of the Ocean Pavilion including initial pressure map (far left) 2D contoured tool path (center) and final 3D design (right) image credit: The Mediated Matter Group

The Ocean Pavilion

The first large-scale construction under the FIM development project and team would be the Ocean Pavilion, a 2.5 meter shading structure fabricated from chitosan, a bioplastic derived from the chitinous shells used and created by oceanic crustaceans. Animals evolved to generate a plastic material spanning large ranges of mechanical properties, from rigid exoskeletal plating to flexible ambulatory joints. For its use in aqueous environments, the material characteristics may be tuned with gradable swelling in water from just a few percent by weight to over 90 percent [12]. A water-based manufacturing platform was developed by integrating a six-axis servomotor controlled robotic arm (Kuka Agilus, Kuka Robotics) with a custom cartridge-fed material extrusion system with digital pneumatic actuation capable of continuously varying extrusion width and density through pressure and concentration, respectively [18]. A design workflow is built around this system, modulating material density, and thereby structural performance, using characteristics of the extrusion process and water-based material. Rather than designing discrete patterns to be printed, a continuous 2-dimensional map of material stiffness is generated based on the structural requirements and then a map

forms. To blur the lines between material interaction and digital design is to exercise in a *post-digital* workspace. The term originates in the arts, an aesthetic based on 'glitches', mismatches and errors between design input and output generated as a result of the oversaturation of digital tools. In the late 20th century music industry, a movement developed around pushing digital instruments past their limits into unexpected and new sounds and musical concepts. Contemporary media artist Kim Cascone describes an "aesthetic of failure" growing in the music design and engineering culture [5].

There are indeed, direct parallels to 'glitch art' in physical design. Experimental architecture and product design projects look for the same edge cases and failure modes in digital fabrication tools. At the University of Michigan's college of architecture, researchers Sandra Manninger and Matias del Campo experiment with their relationship between simple geometric tool paths and unpredictable behaviors in plastic extrusion, Fused Deposition Modeling (FDM) 3D printing. They design Platonic forms, simple rectangular columns, and use a robotic arm plastic deposition system with print parameters (print speed, extrusion temperature, layer height etc.) set outside of the range of typical values and observe how and when the fabrication becomes aberrant, as well as whether that behavior is stable or not. Shown in figure 1-3, by intentionally seeding print errors, they open up a design space of emergent texture and form expressed by process and material interaction superimposed on primitive geometry, revisiting the workflow to achieve such complex texture [37].

1.1.3 Emergent Design of Products

Emergent behavior in fabrication systems offers new space for design, but also brings with it a requirement to separate unpredictability in form from expectation in performance. The ability to build in material information to design workflows greatly increases the potential for diversity of designs, and opens the possibility that emergent aesthetic properties beget emergent performance properties as well. For a product, including at the architectural scale, to remain viable, that performance needs to be accountable at the requisite level for its application. In order to make the most of new design spaces, it will be critical to work on new evaluation procedures for understanding a diverse set of physical products.

Evaluation is required on a case by case basis, but an alternative, systemic approach to performance in emergent design is to compartmentalize

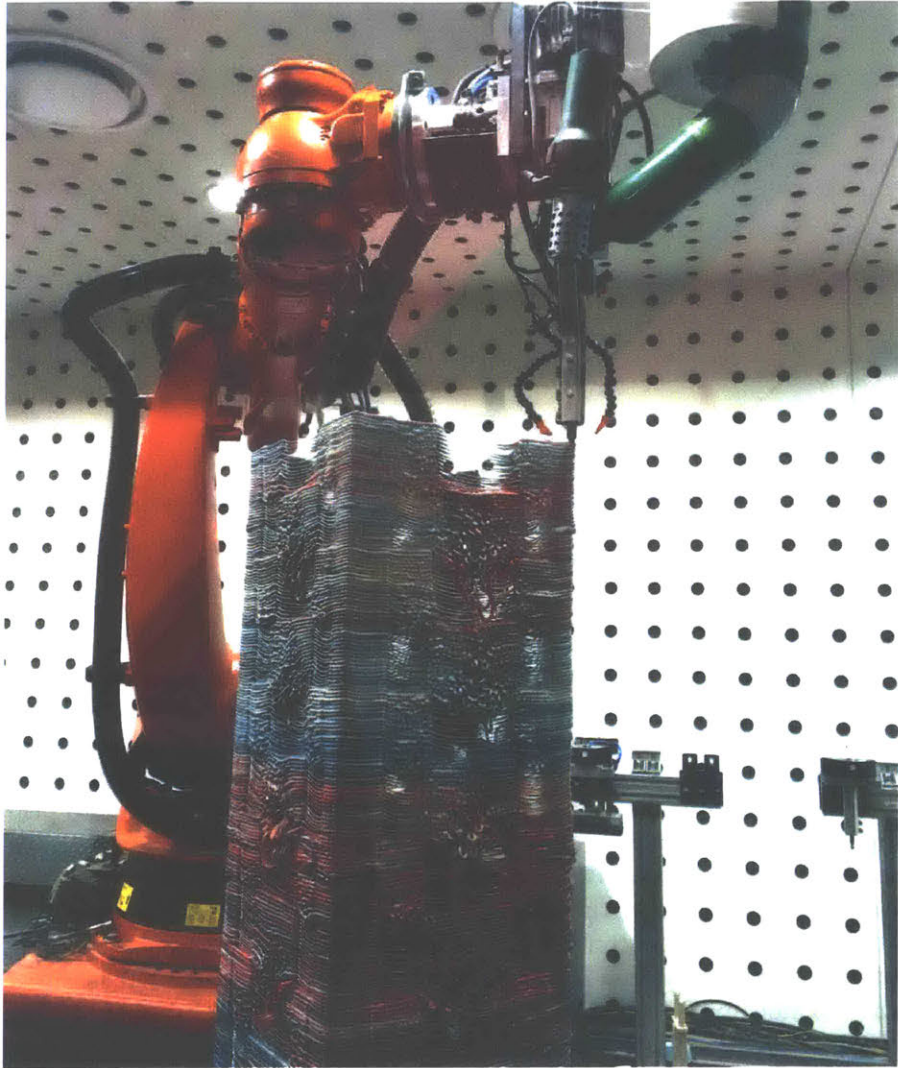


*Figure 1-3: Plato's Columns experimental design project; a robotic arm extrudes thermoplastic filaments in rectangular tool paths with fabrication 'errors' executed through process changes in extrusion speed and pressure
image credit : Manninger and del Campo, ACADIA conference 2017 [37]*



Figure 1-4: *Bad Ombres* product design project; 3D printed clay vases with structure and color gradients
image credit : Emerging Objects

fabrication output into fully understood geometries, emergent geometries, and the transitions between. The Emerging Objects design practice and research group at the University of California, Berkeley presents a series of 3D printed clay vases using this design method [40]. The products display a gradient of color and texture, shifting between functional vessel and flying loop structures (figure 1-4). While the looping forms aren't subject to performative evaluation, the more predictably fabricable solid wall structures can be related to standard clay printing. In order to transition between the two in the design space, the physical transition must also be understood.

Whether seen as uncontrollable and experimental *post-digital design*, extrinsic aesthetic, but non-functional *emergent design*, or material sensitive and functionalized *fabrication information modeling*, the new ecology of material and fabrication is asking questions of how we develop the processes that make products and architecture. It lends itself to materials which have complex or dynamic behavior under fabrication. The water-mediated and time depend properties of chitosan [18][25][22], the unstable deformation of thermoplastics [37], and the malleability of clay filaments [40] serve as precedent for such material systems and accompanying design spaces. Aspects of their design workflows were inspirational to the development of a glass 3D

printing platform, and in the next sections, I outline briefly, the history of glass fabrication and its recent introduction to the additive manufacturing industry, specifically the G3DP system developed by The Mediated Matter Group at the MIT Media Lab and the MIT Glass Lab.

Chapter 2

Motivation: Glass Fabrication from Hand Tools to Industrial Additive Manufacturing

This section describes fabrication technologies for glass from their earliest recorded inventions to the most recent progress in additive manufacturing and is taken from the journal 3DP+ in the article *Additive Manufacturing of Transparent Glass Structures* of which I am a co-first author along with Chikara Inamura and Michael Stern with supporting author Peter Houk and corresponding author Neri Oxman.

2.1 Glass and the Built Environment

Glass is one of the oldest production materials, and its design and production have been slow to change throughout history because of the complex material chemistry involved and extreme working temperatures required. Since the earliest instances of cast glass in 2500 BCE and blown glass in 100 BCE, equipment, formulation, and optical clarity improved via manual production techniques until glass forming processes were industrialized in the early- to mid-20th century [3][11]. Innovations in glass blowing and molding, combined with seminal glass science research, revolutionized glass making, enabling individual production lines to output nearly 10 million containers per year [2] or 2000 light bulbs per minute [3]. In the same period, a new float glass manufacturing process allowed for faster continuous production of flat glass panels [54]. The rate of flat glass production increased by 25 times (a six-fold increase per capita) between 1899 and 2009 [2][1][51][8], and industrialization brought a new wave of affordable glass products with increased performance but also increased homogeneity and decreased customizability. Machine-made bottles, light bulbs, and windows have all contributed to reshaping the world and the built environment.

Since the mid-20th century, glass manufacturing has shifted again, with a diverse group of functionalized products arising from innovations in glass chemistry, including chemical doping for high-strength sheet glass and controlled refractive index for fiber optic data lines. These processes have expanded the applications of glass products but geometries remain simple as the cost of complexity remains prohibitively high. In contrast to the evolving industrial sectors, artisan sectors avoid production investment in large factories and assembly lines and focus instead on tacit material knowledge and sensibility to explore diverse forms and processes. Still, the potential of the inherent material properties of glass, including optical transparency, mechanical strength, and chemical stability, continues to captivate scientists and artists. Recent studies in additive manufacturing of glass suggest possible intersections of both types of sectors, where creativity and complexity are achieved without limitation by quality, performance, or cost.

2.2 Glass in Architecture

Although glass windows existed in Rome by 100 ACE [53], early architectural windows predominantly comprised other translucent materials including shells, minerals, and hide. Even as late as the Middle Ages, stained

glass adorned only the most ornate structures [3][55]. Glass making technologies and applications of glass products evolved throughout the Modern Era, and by the turn of 19th century, glass had begun to appear in substantial parts of the built environment. The Crystal Palace by Joseph Paxton was the first widely hailed example of a fully glazed building system in London, 1851. The structure spanned 71,000 square meters of floor area and required 300,000 panels of plate glass to fully cover the building envelope [7]. Because production of these glass panels actually preceded flat glass technology industrialization, these panels were entirely hand blown and flattened, consuming one third of Britain's flat glass production capability at the time [55].

As of 2015, the global market for glass production was over 200 million tons. Of that, the building sector uses 59 million tons approximately 7.3 billion square meters of plate glass, embracing the low cost and ubiquity of the current industry to populate skylines and allow daylight into homes. Economically, the architectural glass represents a roughly 45-billion-dollar industry [48].

2.3 Printed Glass

Additive manufacturing (AM) was invented over 30 years ago, but only in the last decade has it spread from rapid prototyping to rapid manufacturing (RM), which is defined as the industrial application of AM to fabrication of functional end-use parts rather than prototypes. This shift was driven by a collective effort across disciplines, from engineers and scientists developing improved machines and materials to designers and artists acquiring advanced knowledge and implementing novel applications, such that today, RM accounts for at least 60% of all printed parts. The economic impact of RM is magnified by continued industrial growth, at an average growth rate of 25.9% over the last 28 years [42].

Early examples of 3D printing with sintered glass powder lack the transparency and mechanical properties that the material is prized for, but represent serious attempts to industrialize a glass manufacturing process with complex geometry at reduced cost [52][9]. In recent years, new methods for printing glass have emerged and dramatically changed the process's potential designs and products by enabling the creation of objects with increased geometric complexity, optical transparency, and reliability of mechanical strength.

One major development in sintered glass printing was high-resolution vat

photopolymerization, in which fused silica glass particles are suspended in photopolymer resin and UV-cured into a final form. The resin-glass composite forms undergo a 50-hour debinding and vacuum furnace treatment at 1300°C and 0.005 millibar to remove trapped air and heal cracks. This approach is suitable for fabricating small and highly detailed parts such as microfluidics and optics because it delivers high precision and optical transparency. However, dependency on typical high resolution vat photopolymerization systems limits the speed of this process to glass print rates of approximately 0.02 kg/hr before post processing [36][30][50].

Recent glass printing advancements also include non-sintered processes – for example, Material Extrusion with both solid and molten feed stock. Similar to traditional plastic Fused Deposition Modeling (FDM), a stick-based material feedstock and high-temperature nozzle process was developed by Micron3DP as a means to print detailed glass objects with fine layer thickness. Little technical information has been published, but this similarity to plastic systems suggests a print rate of about 0.05 kg/hr [33]. A limitation of the small filament size is that light scatters as it passes through the printed walls of the object, rendering it more translucent than transparent [39][29]. Alternately, a method for extruding much larger filaments that achieve transparency by using molten material stock extruded through a heated nozzle was developed by the Mediated Matter Group at MIT in 2014 and reported in 2015, and is noted hereafter as G3DP [29]. The first version of this process had a typical deposition rate of 2.2 kg/hr, and build chamber dimensions of 250 x 250 x 300 mm, making it 35 times faster than Micron3DP and 110 times faster than a typical high resolution vat photopolymerization while also achieving optical transparency [23].

2.3.1 Goals for Glass 3D Printer G3DP2

The first phase of glass printer development focused on a proof of concept that demonstrated the feasibility of creating high fidelity optically transparent objects through the deposition of molten glass. The second phase considered a new set of objectives that guided system design, development, and production of parts. These objectives served as a backbone for the research presented in this thesis and are summarized here:

1. Develop a first generation industrial molten feed stock glass filament printer based on the technology previously developed in G3DP.

2. Utilize this industrial glass printing system to fabricate the first ar-

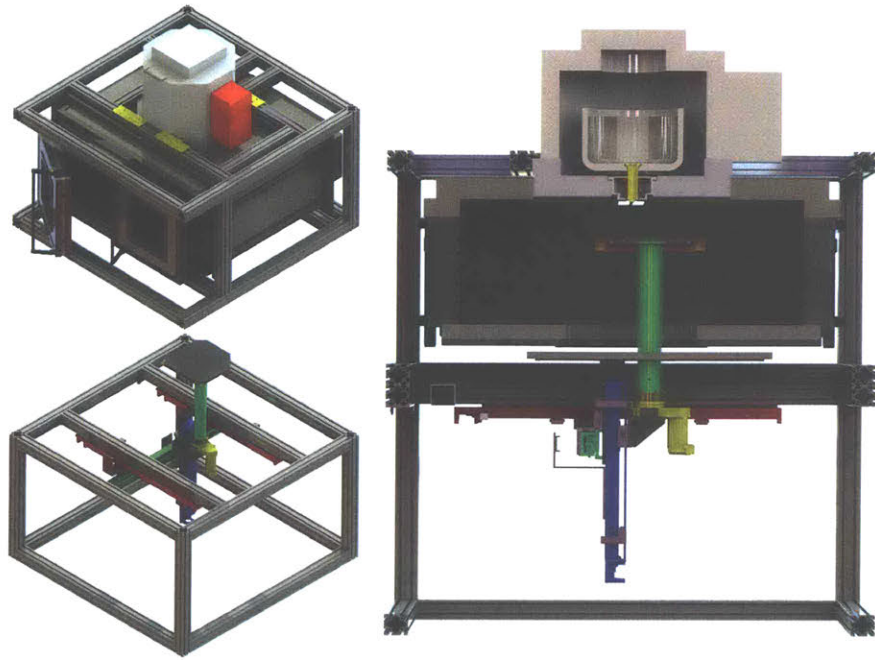


Figure 2-1: Left, shows an exploded view of the upper thermal module and the lower motion control module. Right, shows a cross section of the entire system that reveals the interior detail

chitectural scale printed glass product to showcase the capabilities of the system.

2.4 New Platform - From Prototype to Industrial Platform

2.4.1 System Architecture

The G3DP2 platform is a modular system of two-part vertical assembly: the upper thermal and the lower motion control systems are integrated with a separate control station to enable concurrent development, and independent system calibration to make future upgrades efficient.

The Thermal Control module is an assembly of three independent

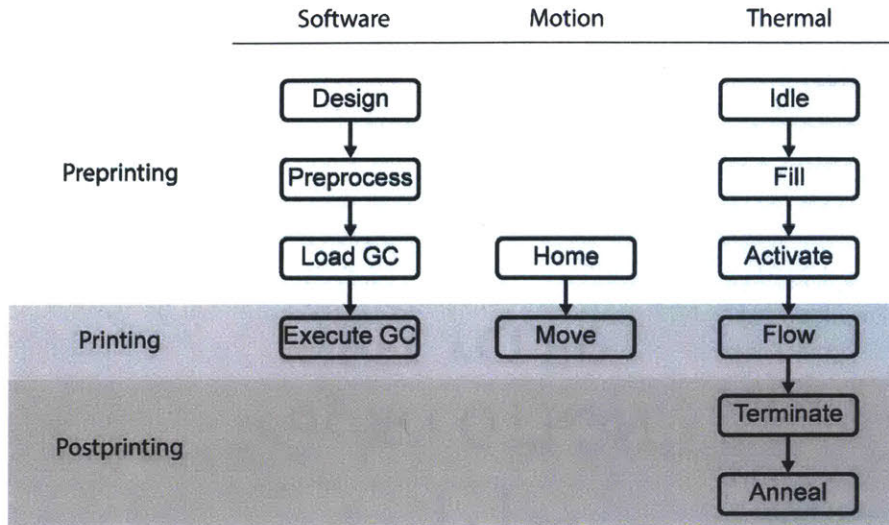


Figure 2-2: Print phases and the corresponding actions of software, motion control and thermal control are shown.

heating systems that are digitally integrated with a centralized control system to provide a continuous temperature profile across the glass transition temperature from melting to annealing.

The Motion Control module is the motion control system, a set of linear actuators along X, Y, and Z axes, and an additional A-axis rotary table with an infinite rotation capability about the Z axis to provide a fourth degree of freedom.

The Control Station is comprised of two independent sets of power electronics and microcontrollers for the thermal control modules and motion control modules. These modules provide a unified access point and control interface to the thermo-kinematic control system of the G3DP2.

2.4.2 Platform Operation

The platform operation of the printer can be divided into the following three phases: pre-printing, printing, and post-printing. In this section, key process steps are examined in software, motion control, and thermal control.

In hardware, the platform is readied. The motion system is homed to re-establish the origin of the system. The thermal control module is kept in an idling mode. In this state, the Nozzle Control Subsystem is set at a reduced

temperature of 800 °C, maintaining an environment in which glass is unable to flow through the nozzle. The Glass Reservoir and Build Chamber are both kept at the standard operating temperature.

The printer is filled with build material for the upcoming print. While idling, the printer can be refilled with either molten glass or room temperature cullet (pre-processed solid glass pieces that are already melted and conditioned from the constituent raw materials). For expediency of operation, molten glass is typically used. The material is transferred from a large auxiliary furnace using a gather ball, a typical glass-casting tool, to the Material Reservoir.

With all other preprinting steps complete, the thermal module of the system can now be readied for flow. This is achieved by increasing the temperature set point of the nozzle kiln from 800 °C to 915 °C. In conjunction, the nozzle gas manifold is activated to heat the nozzle tip. The combined effect of these thermal changes initiates the flow of molten glass. After glass begins to flow, the burner is extinguished, allowing the nozzle to reach a steady-state flow condition.

Printing: After flow has reached steady state, printing can begin. G-Code is sent from the Chilipepr interface to the TinyG motion controller and the build plate begins to move to initialize printing.

Post-Printing: Upon completion of the G-Code file, the printed object is subjected to a thermal soak at 525 °C for about 5 minutes, providing a temperature buffer while it is transported to an external annealing oven. While the Build Chamber in the G3DP2 platform is capable of annealing each print, an external oven is utilized to facilitate the production cycle.

Finally, the flow of glass is terminated by lowering the set point of the Nozzle Control Subsystem back to the idle temperature of 800 °C and by activating the compressed air sent through the ring manifold.

2.5 Towards New Glass Products

The new platform and operational setup represent two years of mechanical development to achieve an industrial scale process for glass additive manufacturing. That process serves as a platform for this thesis, enabling a new design space associated workflow which are described in the following chapter. From the initial improvements from G3DP to G3DP2 in fabrication output, first expressions at large scale, and catalogues of new design vectors to test, I trace the path of this new material-inspired and material-informed fabrication process.

Chapter 3

Design Space

3.1 G3DP and G3DP2

As a systemic development project, G3DP and G3DP2 share a focus in platform, design, and product incorporating expertise from multiple fields including mechanical engineering, materials science, and structural design. This workflow enables the development of a complex iterative tool pulls fabrication information from its own output and deployment. A complete set of goals for machine design are not explicitly set from the outset of development, and therefore a non-linear development path results. Intermediate milestones are roughly positioned but require their own reevaluation throughout the process.

3.1.1 G3DP: The First Stages of Material Information and Novel Design Methods

The G3DP platform was developed with only one explicitly defined milestone, which was to confirm (or reject) the feasibility of additive manufacturing of molten glass. The machine borrowed heavily from standard FDM 3D printers both in machine framework and in mechanical components (as detailed in section 1), combining it with a previously developed technique for glass extrusion, the vitrigraph—literally *glass writing*—kiln system [16]. High temperature components were designed or selected to fit within this framework and a more common plastic end effector or "hot end" was replaced with high temperature glass equipment: the vitrigraph system and a custom nozzle heating system. Critically, these components were required to fit within the (x, y) stage without adding so much mass as to limit its

motion prohibitively. The most complex machine design came in the form of the nozzle and nozzle heating assembly, the component that mates the CNC system to the vitrigraph system, acting in place of a heated metal nozzle that might be found on a plastic printer. Instead the custom designed ceramic nozzle and surrounding heating elements provide flow control very similar to that of a plastic FDM machine, and allowed for the first experiments in glass printed objects.

The objects generated by the G3DP platform were designed based on experience other 3D printing systems and intuition with hand formed glass objects, with the goal to observe, at the highest level, the characteristics of glass printed material. Before considering the functionality of potential products, or even the limits of what might be designed in printed glass, a series of general geometries at multiple scales were fabricated to observe the material and process. This product-agnostic approach allowed for the most reliable fabrication and material information to be brought from experimentation into practice. The question of "what is this platform capable of?" shifts to "how does the material behave during platform motion?". It gives the opportunity for inventors to not only question whether a novel form of additive manufacturing was possible, but to bimodally develop an understanding of feasibility and potential scope. For example, it may have been possible to engineer a system to recreate what are proven to be feasible and marketable plastic 3D printing systems in glass by focusing on matching process characteristics such as print rate, geometric accuracy, and surface finish (layer height/resolution), all of which are generally treated as metrics of quality in standard FDM processes. Doing so might have provided a direct technological context or comparative metric, but would have limited development goals and evaluation of products to that context alone—or at the very least, set a prejudice for the context in which to evaluate the process. Instead, the platform is used to produce an array of testing objects, designed with as few assumptions about functionality or even geometry as possible, and deployed.

Deployment, however defined from research to research (or project to project), is a subtle but critical part of this material-informed workflow. Evaluating the output of a platform is a necessary step—without argument—but requires at least a conceptual performance context. Even selecting evaluation metrics generates assumptions about functionality. In the case of 3D printed glass, questions of structural, optical, and thermodynamic performance all require an assumed context of function, be it structural, daylighting, or as an HVAC component. Making efforts to initially avoid those metrics allows

the research to generate new material information that offers less obvious but equally promising applications. Deployment then is an exercise in self evidence, a presentation of raw material and fabrication information. The G3DP platform exhibition in 2015 is a milestone example, a simple exploration in form or, at a more primitive level, process, in 20 objects, presented as a celebration of themselves, without yet definitions of why or for what. The work was presented to an external audience as a formalized collection, giving a new perspective to the development team. This exercise dramatically altered the nature of the research project. The behavior of glass in this form created a unique and unexpected interaction with light and visual rendering, something certainly not seen in other additive manufacturing platforms. The relatively large filament size, the highly visible curvature from layer to layer, and the complex and dynamic caustics produced offered an entirely new design space based on optical performance that varied widely with printed geometry. These unique properties might well have been overlooked, should the objective have been to chiefly to match metrics for similar platforms. Yet it is based upon this framework celebrating the material behavior and material-fabrication interaction that informed both the design space for the process and most critically, the continued development of the platform into G3DP2, the second generation system that continues to diverge from comparable additive manufacturing processes and defines a novel design and application space for glass.

3.1.2 Lessons From G3DP and Exhibition

Once a novel material behavior is observed which has potential to be the greater design space for further research or production, it opens up and informs the next stages of system development. Through lessons learned from the G3DP platform, a second development system was built to further refine the process and provide a foundation for experimentation into the possibilities of design with printed glass.

For the G3DP platform, the relatively large filament size, often characterized as low resolution, in printing might have been observed as the most rudimentary form of the process that would ever be desired, as most 3D printing systems strive for much finer material deposition. Instead, the optical behavior of the lenticular structure of layered forms printed at this particular resolution presented an unanticipated design space which may be of equal or greater importance to that afforded by higher resolution printing. Continued platform development was based on the current resolution

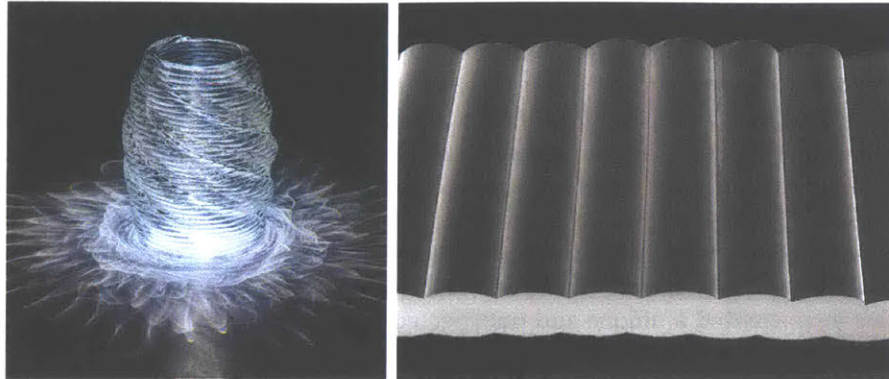


Figure 3-1: glass printed object from the G3DP exhibition (left) and electron microscope image of printed glass layers (right)
image credits Andy Ryan and The Mediated Matter Group

rather than adjusting for greater "resolution". In another sense, that notion of accuracy or resolution is reevaluated. Once the large filament curvature in each layer becomes the intended design, it might be considered as something produced with great resolution and accuracy, but which is produced indirectly of machine control itself.

The meso-scale lenticular nature of low resolution printing was repeatable and scalable to such a degree that it drove development. With large filament size comes a deposition of around 2 kg/hr [44][23], which is extremely high relative to systems of similar build volume and raises a question of scale to the design direction. For the material characteristic of this resolution, what are appropriate scales for products, either singular or part of an assembly, and did the G3DP mechanical platform properly address those scales? For this new space of optical or lighting design, how might scale augment or diminish the desired effect?

In considering scale, we seek to first ask why the material behaves the way it does and how, if at all, the mechanical system is affecting it. In the G3DP exhibit, each of the 20 objects display complex and beautiful caustic light patterns, thanks to this lenticular form of each printed layer. The lens is a result of the viscous nature of molten glass deposited by the machine, the radius determined by the surface tension and allowable range of layer height (figure 3-1). Printed filament dimensions were originally determined by similar glass extrusions, and their dimensions with the intent that the glass would solidify at an appropriate timescale such that deformation of each

layer was small or predictable enough to continue stacking layers indefinitely without dimensional drift (nozzle moving relatively towards or away from parts during printing). As with any fabrication process—experimental, hand-made, or industrial machine settings and parameter were tuned as often as necessary to produce the most consistent results by trial and error. The success of both initial machine design and calibration put the overall process architecture within a range of parameters, including melt, nozzle, and build chamber temperatures, nozzle orifice size, and glass chemistry, where the process is stable. Understanding where that ranges ends requires extensive testing, but to get sense of its extents, we can look at the driving factors for process stability. In the case of 3D printing glass, or any molten material, the greatest driver is dynamic viscosity, the rate at which the material goes from working temperature to solid. Looking at viscosity measurements of both general silicate glasses [4] as well as heat transfer models, we get a sense of how quickly that viscosity might change.

From previous viscosity measurements, both in-project during the G3DP phase as well as literature values [6] we find that temperature changes of 100 of degrees C lead to viscosity changes of up to 4 orders of magnitude. Given the stability of the platform, this suggests that the heating system is of an appropriate scale, to be carried over into future developments. Breaking down filament deposition into a heat transfer model, we know that heat loss from the filament will go with the filament radius squared, a relatively non-linear relationship suggesting changes in filament size would likely have substantial effects.

Further upstream in the process is the pressure required for the extrusion itself. A gravity fed system is by far the most convenient, as it requires no moving parts or active positive pressure systems, both of which are extremely costly—though by no means impossible—to engineer given the temperature of the system. The use of ceramic or platinum auger devices, as well as high temperature pressure vessels is well documented [32]. The pressure is also related only to the height of the molten material in the material reservoir—an alumina crucible—and is described by the relation $P = \rho * g * h$ where ρ is the fluid density (constant), g is acceleration due to gravity (constant) and h is height. The material reservoir (figure 3-2) maintains a constant, shallow change in head pressure in order to keep print rate near constant. Given the pressure in the system at sea level, the desired print rate and bead size are easily achieved. Should the bead size have been desired to be smaller, much greater pressure would be required. Conversely, a small increase in bead size would increase flow rate and print speed dramatically, potentially shifting

the system towards industrial scale output rates.

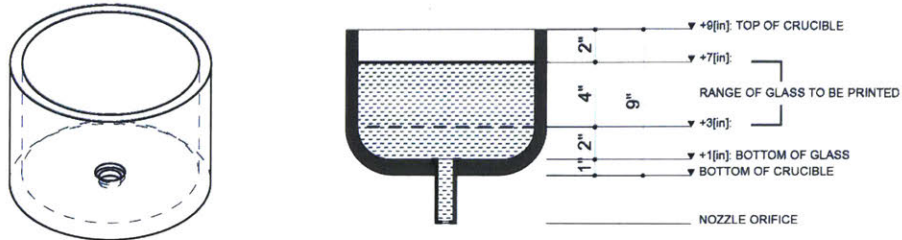


Figure 3-2: 3D representation (left) of G3DP2 crucible and glass height diagram (right) displaying how the reservoir is filled with and emptied of material

To summarize, the current parameters lie in a fairly small range of characteristic flow. Relatively small changes in temperature or bead size dramatically alter flow rate, and potentially require changes in machine architecture. For this reason, a similar thermal architecture and bead size were maintained. Focus was turned to the scale of the system, the scale of the components, the speed at which they could be fabricated, and their potential applications and functions.

3.1.3 G3DP2: platform redesign and description

To evaluate the transition from a prototype system (G3DP) to the industrial system (G3DP2), some key performance metrics are provided as a means of examining the improvements that were implemented. These metrics will be contextualized with respect to the goals outlined in previous section.

G3DP to G3DP2				
Platform	Unit	G3DP	G3DP2	Change [%]
X Axis	[mm]	250	320	128
Y Axis	[mm]	250	320	128
Z Axis	[mm]	300	350	117
Print Volume	[cm^3]	18.750	35.840	191
Glass Reservoir Size	[kg]	2.1	25.5	1214
Material Ratio	[%]	4.6	29.0	624
Process	Unit	G3DP	G3DP2	Change [%]
Nozzle Size	[mm]	10.0	11.5	115
Feed Rate	[mm/s]	6.1	10.0	164
Bead Height	[mm]	4.5	5.0	111
Bead Width	[mm]	9.5	12.0	126
Bead Area	[mm^2]	40	57	145
Print Rate	[mm^3/s]	240	570	238
Flow Rate	[kg/hr]	2.2	5.2	234

Table 3.1: Comparison between the first and second generation of the printer highlighting key metrics. Absolute values as well as the relative change are included.

The first key metric of comparison is scale. An increase in each of the principle axes of the system resulted in a near doubling of the size of the objects that could be fabricated. The mass of the glass reservoir saw an even greater increase, with the ratio of reservoir to print volume rising from 5% to 30% and eliminating the need to refill the reservoir during prints. From an absolute standpoint, this represented an increase in available material by a factor of 12.

The second key metric of comparison is speed. With a minor increase in nozzle size, layer height, and feed rate, the compound effect was a more than doubling in printing rate, making this platform one of the fastest globally,

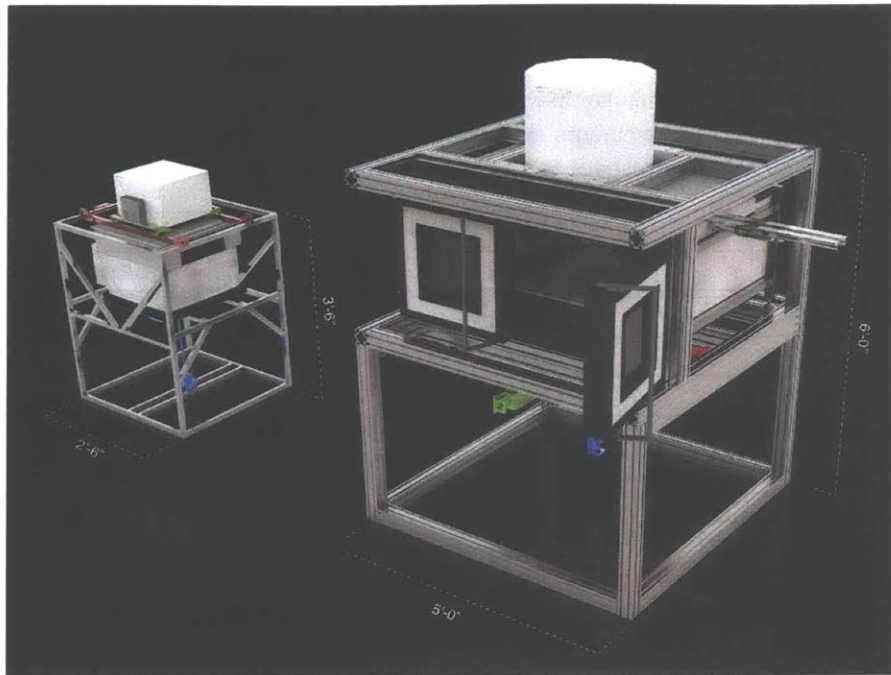


Figure 3-3: The two platforms and dimensions of G3DP on the left, and G3DP2 on the right.

independent of material [33].

The third and fourth key metrics of repeatability and reliability are harder to compare quantitatively with the previous version. Instead, absolute metrics are presented here to show a definitive result for future comparison. Testing of the G3DP2 system indicates the ability to hold positional accuracy to finer than 1 mm and produce a set of circular products that are within 1 mm of the predicted dimensions. Additionally, the new static architecture introduced thermal and mechanical systems that could operate for months at a time without the daily adjustments required by G3DP. Current limitations in nozzle joinery dictate 2-3 week print campaigns, and ongoing research aims to further extend this.

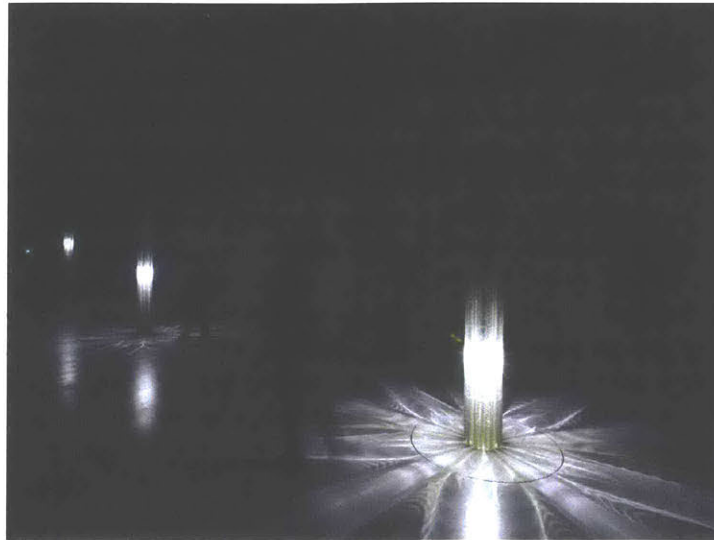


Figure 3-4: 3D printed glass columns displayed during Milan Design Week 2017

3.1.4 Public Installation of Glass Structure, Milan Design Week 2017

Using the G3DP2 technology and a series of preliminary geometrical and mechanical characterizations of its products, a set of three-meter tall structural glass columns were produced for an architectural installation for the Lexus “Yet” exhibition during Milan Design Week 2017. In the new glass design space and material-informed parametric framework, the columns were designed with curvature-dependent methods for geometric morphology, which provided repeatable results in the preliminary design evaluations presented earlier. This repeatability and predictability of manufacturing tolerances strongly inform the derivation of safety and performance factors and the resulting opportunities for design.

The glass columns were structurally optimized within this predictable domain for performance as freestanding cantilever columns with continuous cross-sectional morphology along their height. The cross-sectional profiles at any height are defined by a single constant curvature composed of a network of constant radius arcs and bi-tangent arcs. Along the vertical axis of the columns, that radius undergoes incremental linear change in order to smoothly transition its morphology in both lateral and longitudinal directions, resulting in bifurcating lobe structures. The continuity of morphology prevented stress concentrations at any local point across the structures. The

bifurcation relates structural performance to cross-sectional moment of inertia, with the greatest moment occurring at the point of greatest bending load and continuously decreasing until the point of least load.

Individual columns were constructed from sets of 15 unique printed glass components that were assembled vertically with thin silicone film joinery and steel post tensioning systems to ensure vertical stability. Each column contained a mobile LED light module set on a linear motion system, with illumination controlled by the intersection of the moving light rays and the continuous morphology of the glass structure. This created a dynamic display of large-scale caustic patterns, expressing the incredible potential of glass structures and illumination systems at an architectural scale.

3.2 Forward Development

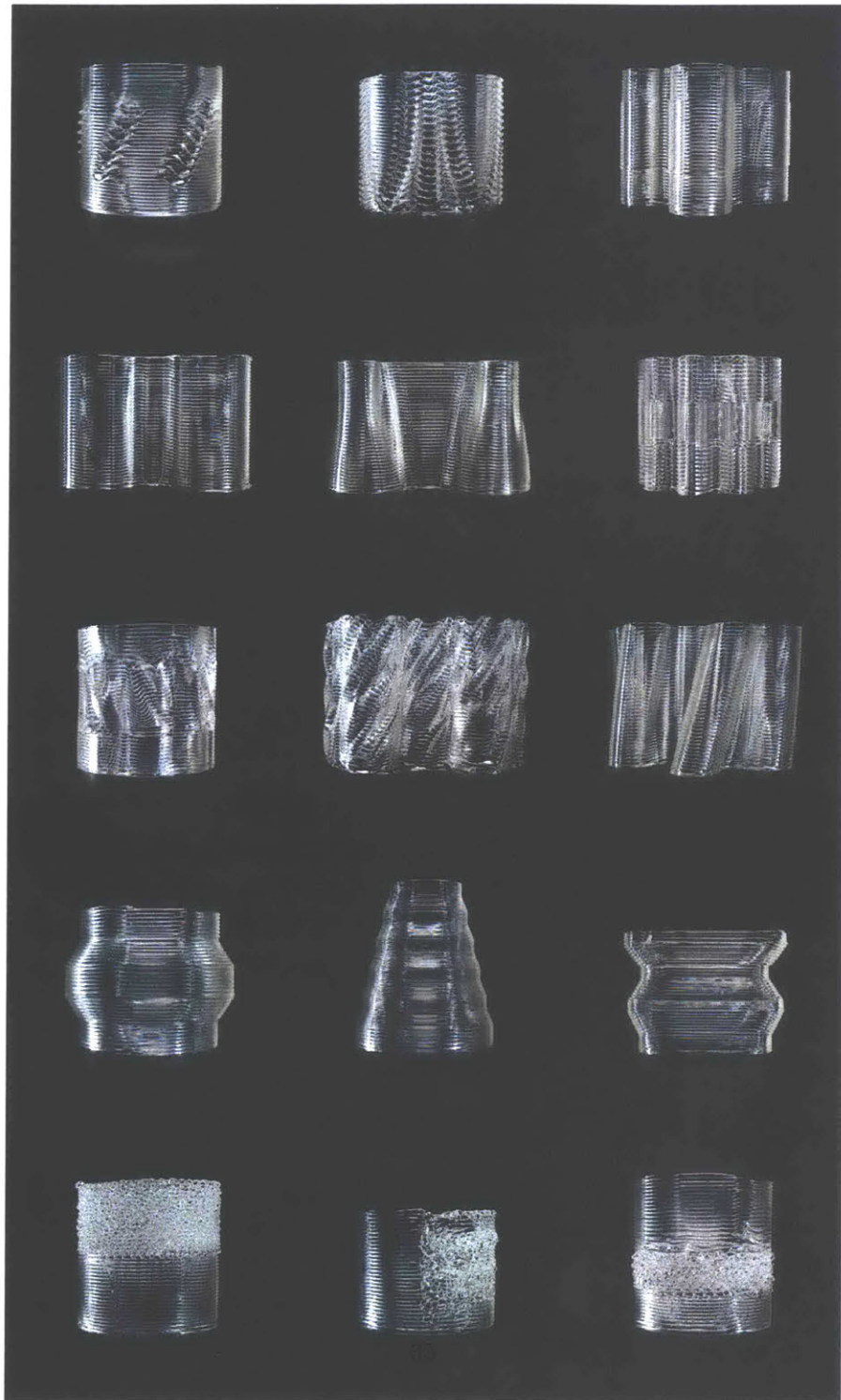


Figure 3-5: selection of glass printed design experiments

One may view the glass column installation as a benchmark in repeatability. Sixty individual components, printed over the course of six months were required to fit within a specific tolerance, post processed and assembled to form continuous structures. Each component was measured and proof tested to ensure not just geometric accountability but minimum structural performance as well. The design of the three columns was intended to leverage the fidelity of the machine, rather than push its geometric boundaries. The scale of each component, 300mm x 300mm x 200mm was well within the available print volume (320 x 320 x 350) and allowed for a smaller change in head pressure from the gravity fed system—and thus, less variation within the print—than would have been experienced from much larger, heavier components, even if they were within the print volume. The draft angle was kept lower than $\pm 20^\circ$; a constraint to the previous glass printer was a maximum draft angle of around 30° . Finally, all components were kept single walled surfaces with no intersections. The design space for such geometric constraints, a single-walled tubular glass shell, remains very rich. The ability to tune the cross-sectional form of a three-meter column at filament resolution 1/600 the scale (5mm) is powerful, and it allowed for the design of continuously morphing structural performance [43] at architectural scale. Furthermore, each individual component was unique in design, *but not in fabrication tool or formwork*, leveraging the flexibility of additive manufacturing systems with the repeatability of the specific G3DP2 machine.

Through understanding the nature of constraints for the G3DP and G3DP2 systems, designers explored geometries that did not push those boundaries. Exploring design in the "safest" possible space not only ensures the success of the installation, but also generates a wealth of data from the machine running consistent, largely unchallenging tool paths, over a substantial period of time and across multiple rebuilds of the machine. It also served as a well-defined baseline for testing different print conditions, methods, and process parameters as something the resulting output could be compared to. As with the first exhibition in the MIT Media Lab, following G3DP, the Design Week installation had its own purpose. From the perspective of platform development it was an exercise in "proof of scale", rather than one of exploring the printed glass design space.

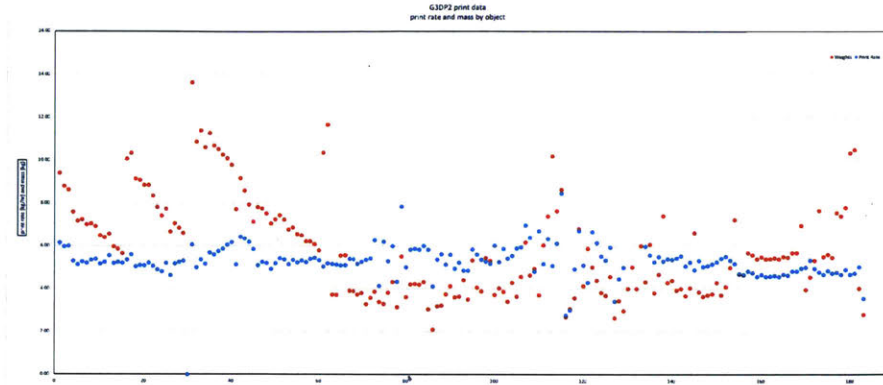


Figure 3-6: print rate in kilograms per hour, shown in blue, and printed mass in kilograms, shown in red, of all printed objects and components from the G3DP2 platform

3.2.1 Tracking the System

A novel material system, glass 3D printing carries no information about general process characteristics or evolution, and requires careful study of its performance over time and with extended operation. The complexity of high-temperature, viscoelastic flow, has required a separation of scales between design input and actual material output. While not completely predictable, the material interactions operate within tolerances of design input and can produce highly repeatable output, but without explicit control at the scale of those interactions. This disconnect in design input scale to material behavior scale makes it difficult not only to understand the behavior itself, but also its relative impact on process evolution and machine wear. For example, we understand that the lenticular structures of glass filaments are dependent on cooling rates and surface tension forces in the molten glass in the interval between exiting the nozzle as a viscous liquid and "freezing" into an amorphous solid, just below the softening point. These forces are self-contained with respect to the design input, reliably producing lens like structures on all objects printed under normal conditions. Designers do not have an explicit or numerical understanding of those internal viscoelastic forces and their evolution. This does not affect the resulting output—such forces operate at a smaller scale than is defined by design—but it does affect the ability to estimate how those forces generate fatigue on the machine

components, for example. And this is also the case for a number of other process attributes including, thermal expansion and gradients, gravity driven flow, and machine stability and vibration.

Finding ways of understanding process evolution, or being able to calculate potential lifetime for mechanical components is critical because mechanical evolution may result in changes which manifest at scales below that of the design input. This necessitates the ability to distinguish whether the change is due to the input or due to the evolution of the machine and without explicit knowledge of the forces acting on the machine. Often this understanding can be achieved by the careful analysis of data generated by production output.

Even the simplest characteristics in output can be aggregated into an informative dataset. A simple, but fundamental characteristic of an additive manufacturing platform is the mass flow through the system, the *print rate*. Every object printed using G3DP2 has a known mass, and when coupled with the known time it takes to complete prints,¹ enables an understanding of flow. The print rate is calculated as the former divided by the latter per print, mass per unit time *kg/hr*.

Figure 3-6, at the opening of this chapter displays the printed mass *kg* and print rate *kg/hr* of every object printed with G3DP2. A wealth of data, it highlights the diversity of print conditions and outputs, and upon inspection, many trends and critical points begin to appear. Over the last two years, there have been numerous print campaigns with varying objectives, including experiments whose purpose was to test different print rates, which substantially complicate this chart, but coupled with information about the history of printer and objectives of experiments, it becomes distinctly informative. In this section I will explore several of characteristics of machine and process evolution through sections of this data map.

Consistent Printing : Glass Columns

The most apparent trends are noted in the leftmost section of the plot, four distinct negative slopes, now isolated in figure 3-7. These represent the four columns (three which were displayed, one which served as a back-up) which were printed for the Milan Design Week exhibition. As discussed in

¹while this system, as most off the shelf 3D printer software packages, is not particularly accurate, it is consistent, and by manually recording the time for a number of prints, we are able to say with great certainty the print time of any object based on the software estimate

section 3.1.4, the columns were designed with continuously morphing cross section, where the curvature and path length decrease from the bottom to top. The columns were fabricated in this order as well, so we see the mass of each component, shown in red, from greatest to least in four roughly linear slopes. Given the predictability of the recorded masses, we might expect to see the same in recorded print rate. Indeed, we see an average print rate of 5.3 kg/hr, and a linear regression of the data gives a slope of 0.0004 kg/hr/component, strongly suggesting no major evolution in print rate over the course of column fabrication.

While the data is globally consistent in rate and mass, there are certainly outliers that warrant further examination and are best revealed by dividing the plot into the eight campaigns across which the fabrication was completed (figure 3-7 bottom). A *campaign* is here (and generally in the glass industry) defined as a production run during which a glass printer or furnace is kept at operating temperature. As many of the components that come into contact with molten glass cannot be reused after the system is cooled to room temperature, the machine is brought to working temperature and maintained until production is halted by a mechanical breakage or when the production goal is reached. These campaigns may last from a period of days to several weeks², but in between, all consumables are replaced, namely the nozzle and crucible, and the components are rebuilt as needed and refitted. By observing the output from campaign to campaign, we can get a sense of how the tolerances in those machine components, or differences in their installation may affect the printing process. Detailed recordings of the rebuilding process and geometric variability of components is also critical to those comparisons, and so the refitting process is documented with video and photo, and dimensions of components recorded for every campaign.

Looking across the plot in figure 3-7 (bottom), the sections shaded alternately denote the different campaigns during which each component was printed. The first three objects show a distinctly higher print rate than the next twelve, though all are part of the same column. These three were printed several months prior to the next twelve as part of a different campaign. Just looking at these three data points, we also note that the object masses (in red) lie slightly high for the trend in the rest of the column. This suggests the printer set-up for this earlier campaign to intrinsically have a slightly higher print rate than the latter, calculated at an average of 6.1 kg/hr compared to 5.3 kg/hr, an increase of 15%. The print rate for the later

²due to the probabilistic nature of some breakages

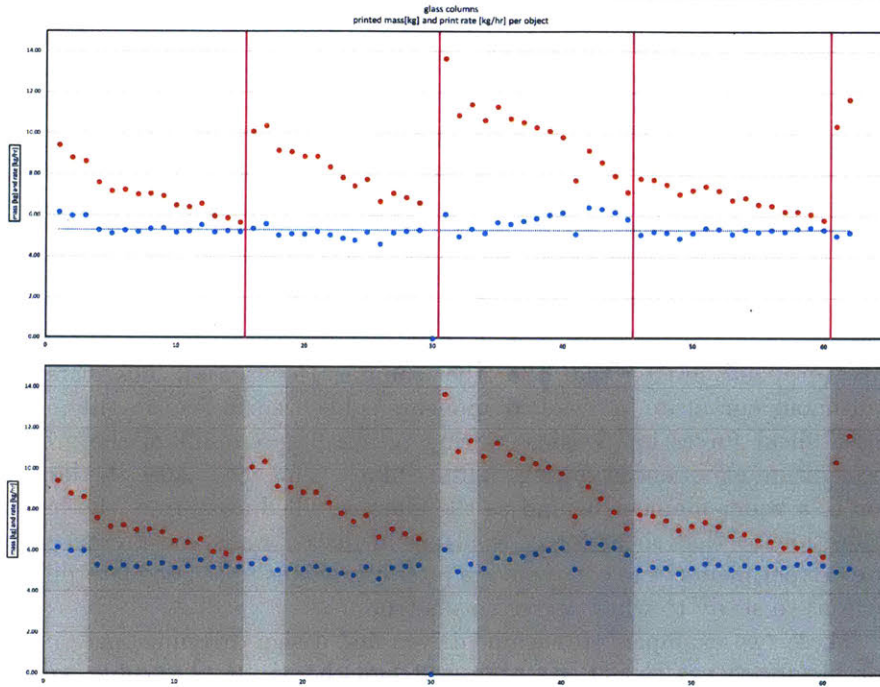


Figure 3-7: isolated print rate (blue) and printed mass (red) of glass printed column components by object divided by column in magenta lines (top) and print campaign in shaded regions (bottom)

campaign also matches exactly the average print rate for all component production. This discrepancy, narrowed down to printer setup, is believed to be a result of differences in thermal system control including exact placement of thermocouples. A control offset of this nature would cause the machine to run at slightly higher temperature, slightly lower viscosity, and therefore higher print rate.

While print rate deviation can be explained by different machine char-

acteristics, data analysis may also reveal trends in how the design of printed objects can affect printed output. We look back at figure 3-7 (top), to examine print rate between columns, all of which had slightly different designs (barring column 4, a backup copy of column 1), and are separated in the figure by the vertical magenta lines ³. Discounting the first three points as outliers, the average sample standard deviation [17] in print rate (blue) for columns 1, 2, and 4 are 1.1%, 2.7%, and 1.3% respectively, while the average deviation for column 3 is 7.3%. All but one of the column production runs spanned multiple campaigns, so rather than looking for differences in machine characteristics, we hypothesize that the difference is due to the difference in design input, something which is affecting the print condition and thereby, the production output. The column exhibiting the greatest deviation was designed with the longest cross sectional path length and highest curvature, 20% greater than the other columns (figure 3-8). The increased continuous curvature in these components is believed to lead to greater induced shear forces in the glass during printing as a result of the greater acceleration experienced during tighter curves. This may cause the deposition of a wider filament behind as the glass is pulled away from the line of deposition by that shear force, resulting in thicker walls and greater print rate. Experiments were conducted in later campaigns (discussed later in this section) to study to what degree this is true.

These two examples of machine driven and design driven changes in expected fabrication output are both still hypotheses. It is possible, surely, to explain them with entirely different theories, thanks to the complexity of machine and material interactions, but they highlight the importance of even simple data collection when dealing with such systems. A point as simple as mass or print rate, can show consistent trends which at the very least point to which process parameters or design factors should be studied in greater detail, and at best, provide convincing explanations for differences in output and possibly even methods for control over those differences. A process like glass printing, with self-contained material interactions which are not designed explicitly, will inevitably output something which is a product both of material/machine iteration and of design. Without explicit control over the former, it is impossible to know before production what the resulting form will be influenced by. In looking at trends in the data, those relationships can be better understood.

³the last two data points are reprints of parts in earlier columns which were deemed defective

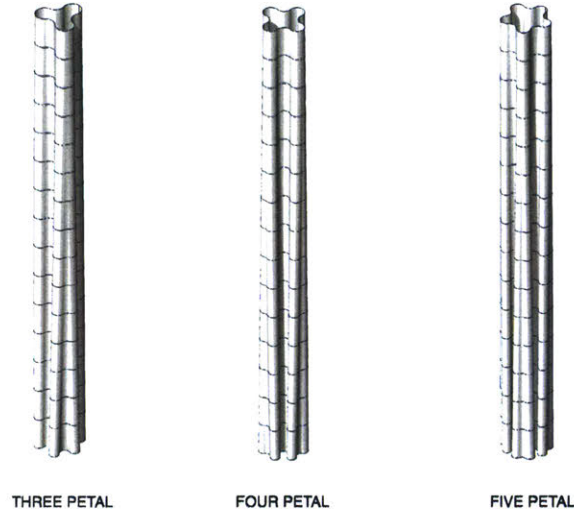


Figure 3-8: surface models of 3 types of glass printed columns: 3-petal and 4-petal designs have maximum radius of curvature 60 mm while the 5-petal design has maximum 45 mm
 image credit : The Mediated Matter Group

Inconsistent Printing : Process Experimentation

Transitioning from observed data trends in glass printed output to tunability of output by design means intentionally disrupting those trends. Over the course of this research, a number of different experimental print designs were conducted, reported in detail in the next section, which intentionally altered print conditions in such a way that we expect to see very different process output characteristics. Figure 3-9 shows the mass and print rates for 121 glass printed objects, design experiments conducted after the fabrication and installation of the four columns. Data points in green identify these experiments as ones with process-altering designs. Variations in layerheight, print speed, and print condition, were all tested to observe how design input would alter fabrication output, and so are called out in the global print mass/print rate plot. These data points are expected to have print rates that differ from the norm. Mass data for the experiments remain presented in red—as object mass is object dependent—but print rate data for experimental objects is presented in green. Many other objects printed during this period were designed without such process-altering characteristics, so their print rate data remains blue and is used as a comparative baseline.

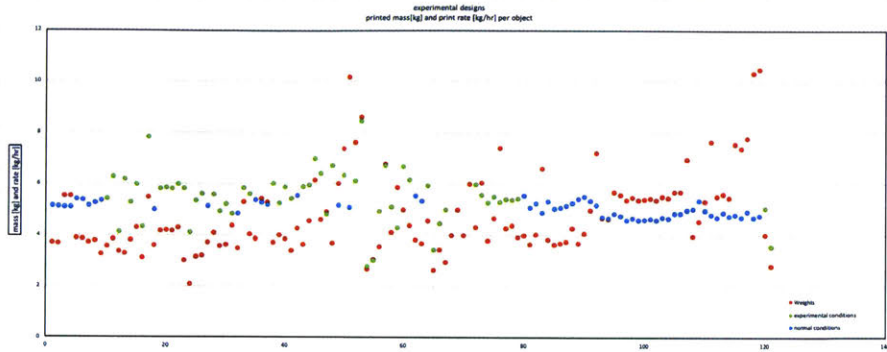


Figure 3-9: print rate (blue and green) and printed mass (red) of 121 experimental and test objects printed between June 2017 and January 2018

The linear regression for these remaining data points matches closely that of the column production campaigns and the global trend with a nominal slope of $-.004 \text{ kg/hr/component}$ and an identical average print rate of 5.3 kg/hr . This suggests that during these campaigns, the printer setup was within measurement tolerance to the global average, and geometric data from the intentionally outlying experiments may be compared to that baseline, and related directly to the design input. Without the global dataset, however, it would be impossible to denote to what extent the geometric changes are a result of the design or a result of the machine and material.

Transitions : Machine Rebuilds and Campaigns

Along with observing trends in consistent print conditions and output, or identifying intentional changes in process as outliers in the collected data, we can also look for transitions in data trends or non-trends, as a further means of studying process evolution. Figure 3-10 isolates the print rate data from the previously shown 121 design experiments, and separates object data by campaign using the magenta lines. In the section plotting the third campaign we observe distinct trends in print rate which have very clear transitions. For example, at object number 85, we begin to see a steep increase in print rate over the next 5 objects, and then a drop after object number 90 until number 94, where we see a relatively consistent plateau. The observation of transitional data like this again brings up question of and potential insight on the evolution of the process. In this case, the design information about

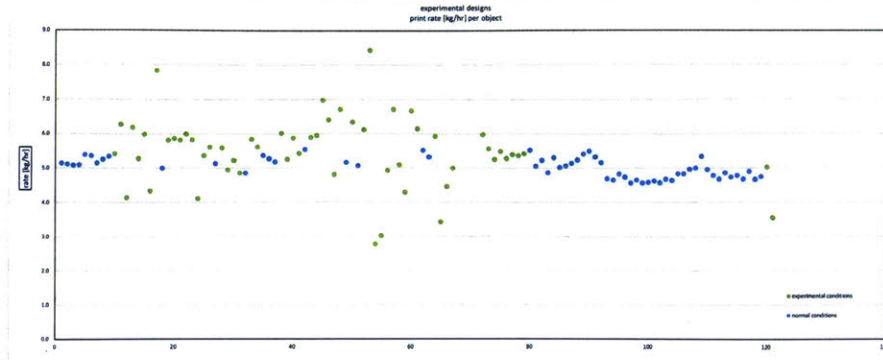


Figure 3-10: print rate in kg/hr of standard print condition experiments (blue) and altered print condition experiments (green) by object

these 9 objects tells us very little about why such a transition might occur. They do not have a consistent increase in any condition which might affect print rate, nor are there documented changes in printer operation. Future comparative study of the geometric features of the objects in question, as well as more detailed operational reports, may shed light on the causes for such deviations.

Data collection and observation may serve another useful purpose which would be to identify signs of current or incipient failure resulting in evolution of the thermo-mechanical system. A sudden decrease in print rate might signal an electrical failure or even a material leakage around the heating systems, resulting in higher viscosity. For this exercise, the entire history of the G3DP2 machine and process is being analyzed, and while hindsight may help explain details previously unnoticed, it currently remains academic. There is little justification for making concrete claims about the factors that affected the system in specific instances, but a catalog of incidents and potential explanations is a valuable resource for future development.

3.2.2 Future Machine Information and Tools

If the data can be collected close to real-time, updated during or after every print, and incorporated into a growing dataset—as opposed to the multi-year aggregate we are analyzing postmortem—trends, outliers, and transitions can be much easier to identify, plan or design accordingly for in order to further enhance fidelity of printed objects. A live tracking of print rate might be able to automatically adjust print speeds during a campaign, either increasing speed to account for greater material flow than expected or slowing

down to account for the opposite. A common feature on many consumer 3D printing platforms is a feed rate override control allowing the user to finely adjust print speed during a print if it appears that the machine is over/underextruding. While it is difficult to observed the subtle differences in the transparent objects during printing, data collection over increasingly long operational periods will only offer more insight on what changes can be made to increase consistency of output.

From this high level view, we've looked at how the platform operates with an agnostic eye. An analysis of the global dataset allows for a holistic understanding of process development and output, a critical exercise when that process is so dependent on complex or unpredictable material interactions. Without a predictive model incorporating accurate values for temperature, viscosity, and mechanical forces in the system, it becomes necessary to closely examine the output under recorded conditions in order to form degree of predictability and therefore a material-informed repeatability under different conditions. The next sections provide greater detail into experiments which attempt to change those printing conditions and record the response in glass printed products. These experiments were discussed here as outlying data points, measured against the baseline of a wealth of glass printing data, but will now be expanded as their own empirical data collections.

3.2.3 Feed Rate and Layer Height

There are a few fundamental process characteristics that define an additive manufacturing system and are linked to the nature of AM. For a material extrusion system, material selection, layer height and path width, and feed rate (the speed the printhead moves relative to the substrate/object), answers the questions of, in a very basic sense, what is being added, how much or how little the machine adds it at a time, and how quickly that addition can be accomplished. As discussed in sections on the development of G3DP and the first architectural scale installation that made use of G3DP2, these values were kept constant or incrementally increased. The systems both used the same soda-lime glass formula (Spectrum Glass system 96). The glass deposition dimensions were slightly increased from G3DP to G3DP2, from layer height 4.5 mm and width 9.5 mm to 5.0 mm and 12.0 mm respectively. feed rate increased as well from 6.1 mm/s to 10.0 mm/s, as a measured response to greater volume of material feedstock and greater head pressure in the gravity fed system. For the G3DP phase and until this experimentation phase for G3DP2, these values went unchanged for the sake of consistency with a process that is very sensitive to process changes.

After manifesting prototype objects and architectural constructs in printed glass [34] under standard conditions, we began to explore how changes in layer dimensions and feed rate would change print characteristics, as well as understand the feasibility of smaller or larger layer height and faster or slower feed rate. These would have implications in the visual characteristics of transparent layered objects and production output speed and volume.

Test Object Design

While the geometric and mass information from previous print campaigns was useful for understanding a general baseline for the process, for a more direct comparison of print conditions, a custom test object was designed with sections of normal printing conditions (control) and sections of experimental conditions (experimental), so as to be comparable within the same part. A starting geometry for part was a cylinder of diameter 200 mm and height of 40 printed layers (nominally 200 mm). It is necessary to designate the height of the component in number of layers rather than units of distance because the experimental print conditions specifically involve printing taller or shorter layers. The bottom 10 and top 10 layers are kept as standard to ensure consistent print initiation and termination, as well as allow the

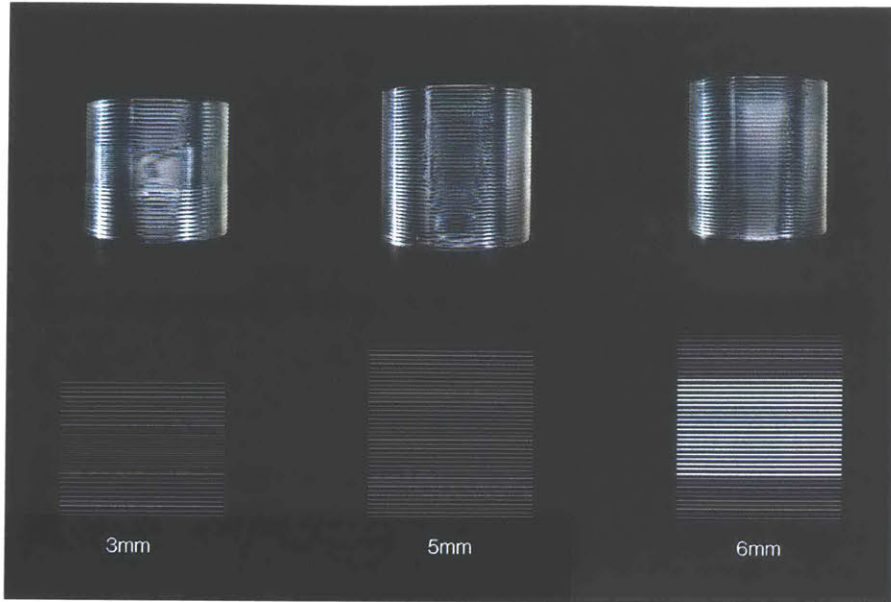


Figure 3-11: 3 examples of layerheight experiments, varying height in the test section (middle 20 layers) from 3 mm, left, to 5 mm, center, and 6 mm, right; below, the experiments are represented graphically with scaled layer thickness and total height

process to reach a steady state⁴, and the middle 20 layers were utilized for testing with different print conditions. Figure 3-11 shows a layering diagram for three example test objects with varying layerheight from 3 mm to 6 mm. Along with full changes in print parameters, the design also allows for patterned changes, back and forth between control and test, shown in figure 3-12.

⁴small differences in build substrate or temperature can cause inconsistencies in the first few layers, but are usually recovered once printing temperatures and dynamic adhesion reach an equilibrium. These errors don't cause print failure, but when testing new parameters, we sought the most consistent control condition possible.



Figure 3-12: feed rate experiment with half of each layer in the test section printed at double the control feed rate (20 mm/s)

List of Experiments

Feed Rate and Layer Height				
object #	feed rate(s) [mm/s]	layer height [mm]	printed mass [kg]	print rate [kg/hr]
control	10	5	n/a	5.3 (avg)
1	8	*	3.38	4.1
2	12	*	3.58	5.4
3	14	*	3.86	6.3
4	20	*	3.30	6.2
5	*	3	3.52	4.9
6	*	4	3.14	4.3
7	*	6	4.20	5.8
8	*	7	4.32	6.0
9	6	7	5.32	5.8
10	*, 8, 14 alternating	*	3.50	4.9
11	*, 20 alternating	*	4.02	5.3
12	*, 20 half layer	*	3.4	5.4
13	*	3, 6, alternating	4.62	6.4

Table 3.2: list of feed rate and layer height experiments (* denotes value is equal to control)

Results and Visual Output

These experiments in varying layerheight and feed rate first confirm an extended range of print parameters. A minimum of layerheight 3 mm and maximum 6 mm were printed without any sign of print failure over 20 layers. A maximum feed rate of 20 mm/s, double the control feed rate, was also established, which would halve print times in a production process. However, faster printing dramatically changes the flow characteristics, depositing much narrower path widths. This results in a print rate of 7.1 kg/hr compared to the control rate of 5.3 kg/hr, and is clearly visible in the object displayed in figure 3-12, where half of each layer in the test section was printed at 20 mm/s.⁵

feed rate and layerheight experiments also revealed this resulting optical distortion, as a new design vector. A 20% difference in layerheight or 100% difference in feed rate generate visibly different optical behavior from the control print condition. Small changes in filament dimension affect the

⁵7.1 kg/hr is the calculated rate for the 20 mm/s feed rate. Because it is only printed at that rate for 20 out of 40 layers, the object's total print rate is 6.2 kg/hr, as reported in table 3.2.

curvature and scale of the lenticular cross section of each layer, which has a much greater effect on visual appearance but without compromising the object's overall structure. Beyond a purely aesthetic design vector, further analysis on the light transmittance and image rendering properties will be useful in understanding how the available range of glass printing parameters can be tied to optical performance. A brief exploration into that optical performance is presented in section 4.2.2.

3.2.4 Curvature, Draft Angle, and Free Path Printing

layer height and feed rate are the fabrication parameters that describe or dictate the characteristics of deposited glass filament. Increasing in scale, we also experiment with the effect of object-scale geometry (300 mm x 300 mm x 300 mm at the largest) on printed output. Feed rate and layer height are one-dimensional parameters, yet inherently, global geometry is three-dimensional and cannot be captured by the previously described test object. Instead, more comprehensive testing designs are required to characterize different geometric forms. The forms that were explored in this experiment set fall into three categories

1. curvature : range of local wall curvature in the horizontal (x, y) plane of an object.
2. draft angle : the local wall overhang angle off the vertical (z) axis
3. free path printing : filament deposition in free air, not on top of previously printed layers

In the previous phases of the project, which focused on proof of concept (G3DP) [23] and architectural scale production (G3DP2) [34], geometric constraints were strictly imposed to ensure repeatable and consistent fabrication. An intuitive sense of the process, gained through having a hand in its development, informed what constrained the design, and the effort to design fabricable objects and components was largely successful. A publication on the first glass printing prototype reported a maximum draft angle of $\pm 40^\circ$. At this stage, the focus was on output rather than an expansion of the design space. .

Here, though, a careful approach is needed to understand the relationship between the glass process and its geometric output. Each test component is designed to be an incremental shift in geometry, often combining multiple



Figure 3-13: (left) multi-radius large and (right) multi-radius small experimental object

geometric elements to test for general feasibility before generating a battery of tests at higher design resolution.

Test Object Design : Curvature

The glass printing process is tied very closely in mechanics and aesthetics to curvature. The material behavior is dependent on the fluid and viscous nature of molten glass, which dynamically responds to changes in motion and is influenced by surface tension and shear forces. Both of these physical interactions make it difficult to generate sharp angles in glass—whether digitally fabricated or blown by hand. The minimum radius of curvature generated by controlled printing that is possible is half the width of a single glass filament (for G3DP2, 5 mm). The viscosity of glass causes a delay in response to motion, so the true minimum renderable curvature must be greater than this, but taking a 5 mm radius of curvature as a minimum, it is still 1.6% the scale of the largest printable object. Given this relatively large magnitude of minimum curvature, it is integral to each full scale design and one of the drivers of the design space overall.

Searching for the true minimum radius of curvature (maximum curvature, which is described as $1/R$), then, is only part of the objective in curvature analysis. When even the smallest curves become part of the design, the entire range becomes relevant to design. Taking this into account, two

curvature-specific test objects were designed to test a range of different values within a single object. Designated, *multi-radius large* and *multi-radius small*, the designs were extrusions of a set of bi-tangent arc pairs, in a range of radii, both in positive and negative curvature. The radii in the larger design ranged from 20 mm to 60 mm and 10 mm to 15 mm in the smaller component. In order to explore not just the effect of different curvature on the printing process, the multi-radius objects were also integrated with the previous layer height and feed rate experiments. Using the same formal testing method as before, the center 20 layers of each multi-radius object also serve as canvas for testing layer height and feed rate conditions.

List of Experiments and Results: Curvature

object #	Curvature		
	min radius of curvature [mm]	max radius of curvature [mm]	superimposed condition
1	15	60	
2	10	15	
3	15	60	+100% feed rate
4	15	60	-40% layer height
5	10	15	-40% layer height

Table 3.3: list of curvature experiments with radius of curvature ranges and cross references with other experiments

The multi-radius objects showed a degree of stability in printing even at the tightest radius of curvature for 40 layers, though there was noticeable deviation from the intended path in the smaller radius object. As the nozzle itself traces the exact curvature from the design, aberrant behavior often results in layer path width changes during tight turning radii. The multi-radius small object varies in layer thickness from 12 mm to as much as 19 mm at the tightest corners. This can be explained by the high viscoelasticity of glass making slow to respond during such changes of direction. Viscoelastic response is non-linear with respect to acceleration. Acceleration of the material does not increase as quickly as the force applied to it, so while the nozzle moves at a constant rate along its path, changing direction quickly applies high shear forces to the glass, which won't accelerate as quickly at the nozzle. While not a catastrophic failure to print, this would be described as a failure to render design to the normal process tolerance.

In combining the multi-radius design with the previously experimented 3 mm layer height (-40% from control), both mulitradius small and multi-radius large objects displayed errors within the test section. Periodic ripple-

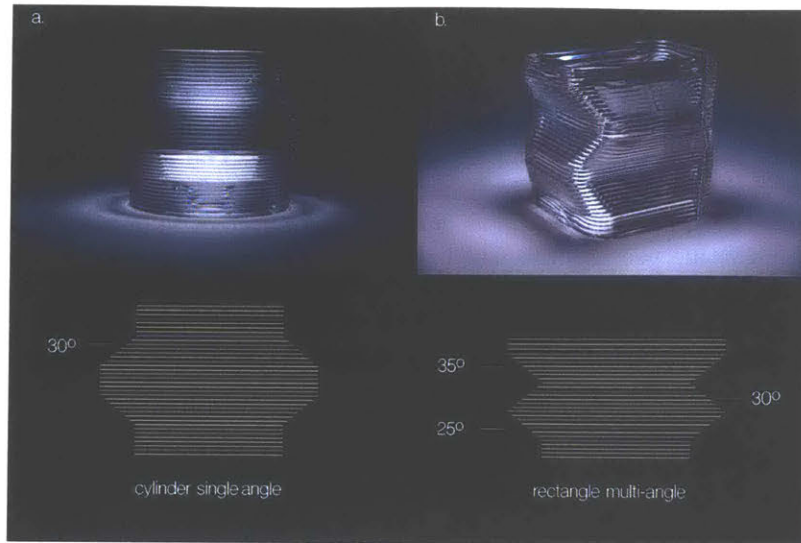


Figure 3-14: examples of cylindrical (a) and rectangular (b) draft angle experiments; below, the two experiment types are represented graphically displaying single and multi-angular sections

like effects can be seen on the smallest radii of the large part and around all radii of the small part, a result of printing just beyond the threshold of stability. While not a catastrophic failure to print, the results show a deviation from design and a change in surface finish.

Test Object Design: Draft Angle

The test object for draft angle was designed to only test a single representative angle at a time. Shown in figure 3-14a, the object is divided into three straight cylindrical sections joined by the two angled test sections. This test explores both a draft in the same direction as accretion of print motion (towards the center of the cylinder) and in the opposite direction. Upon completion of cylindrical draft angles, a second set of test objects was designed to test both flat and angled drafting behavior. Shown in figure 3-14b, a rectangular cross section morphs in and out, again testing positive and negative draft in a single vertical plane. These tests also accommodated three different draft angles in a single component. As with curvatures, layer height values were subjected to integrated testing with draft angle. A 3 mm layer height object was produced for the type A draft angle test and both a 3 mm and 4 mm layer height object were produced for the type B test.

Draft Angle		
object #	draft angle [$^{\circ}$]	layer height [mm]
cylindrical		
1	30	5
2	35	5
3	35	3
rectangular		
4	25, 30, 35	5
5	30, 35, 40	4
6	35, 40, 45	3

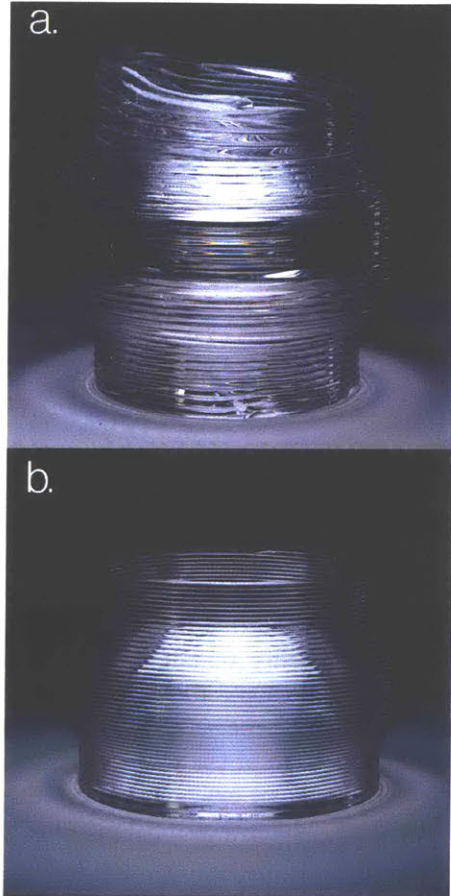
Table 3.4: list of draft angle experiments and cross references with other experiments

List of Experiments and Results: Draft Angle

Initial experiments in draft angle found a point of failure and a real constraint in cylindrical draft angle. The first test at 35 degrees produced a critically unstable print condition, resulting in geometric failure of printing by the end of the 40 layer object, shown in figure 3-15. Under normal print conditions, the slow cooling rate for glass results in the viscosity remaining relatively low for a time after the material is deposited, and causes the glass to settle from the cylindrical orifice shape into a lenticular shape. As long as this is consistent, it can be accounted for, but when enough of the glass overhangs from the previously layer, it is observed to cause an exaggerated settling effect, and the nozzle offset effectively increases indefinitely, until printing is no longer maintained.

A draft angle of $\pm 30^{\circ}$, however, does not exhibit this divergent behavior and can be reported as the maximum drafting angle for the system with this glass formulation and our standard print conditions.⁶ The draft angle relationship is dependent on the post-deposition settling, and so a test object with draft angle $\pm 35^{\circ}$ and layer height 3 mm was shown to be a stable condition (figure 3-15 b). The thinner layers in this object cool much faster and deform much less than the control thickness of 5 mm, allowing for consistent printing at steeper angles.

⁶The viscosity curve and softening/freezing point is heavily chemistry dependent so while the artisan-tailored glass used by G3DP2 (System 96, Spectrum Glass) freezes at this rate from this temperature, a glass formulated to set up much sooner would likely achieve greater overhang angles



The rectangular test objects were designed to test a range of different planar (as opposed to cylindrical) draft angles ranging from $\pm 25^\circ$ to $\pm 45^\circ$, leveraging the ability of thin layers to achieve steeper angles. All three layer heights tested, 5 mm, 4 mm, and 3 mm, exhibited stable behavior. However, similar to surface finish deviations observed in thin layers under small curvatures, a rippled pattern error is observed around the transition points on the 4 mm and 3 mm layer height tests. An interesting byproduct of this was the crack development around the corners of this part. It is hypothesized that transitions in thickness around the sharp corners and resulting thermal stresses induced between the relatively thin walls and relatively thick corners contributed to crack formation.

Figure 3-15: settling error in 35 deg, 5 mm layer height draft experiment (a) and successful 35 deg, 3 mm layer height experiment (b)

Test Object Design: Free Path Printing

A feature not commonly described with processes oriented towards high fidelity rendering of design input is the ability to deposit material at a 90° or "complete" overhang, referred to here as *free path printing*. While there are materials capable solidifying quickly enough to completely print in free space, including extruded plastic [13], arc-welded metal [24], and quick expanding sprayable foam [35], in every case, the lack of a constraining substrate alters the behavior of the material when compared to standard print conditions. In some examples, it's a non structural aesthetic or design feature [37] and is an exercise in emergent design, discovering new ways of forming material where modeled object is not expected to match the output, and is often not suitable for use within the structure of an object. This is the case as well for free path glass printing.

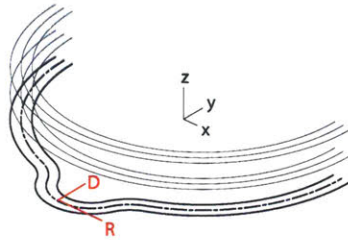


Figure 3-16: diagram of hoop-like free path printing tool path. The hoop extends away from the previous (not shown) and next (above) layers by distance D and is scaled by radius R

The molten glass used by the G3DP2 platform takes tens of seconds to solidify below the softening point, far too long to be able to continuously print in free space, so a design method was developed for printing slightly away from the previous printed layers to produce limited length flying structures that behaved partially like a discrete region of high overhang. The result of this was found to be an altered surface finish. In this method, a continuously curved section or *hoop* is generated in the tool path of specific radius R and radial separation D from the previous layer (figure 3-16). While this is displayed as a planar hoop-like feature in CAD, it generates a solid, drooping overhang as the glass relaxes and joins previously printed layers. A battery of test objects were designed, altering the radius value for the hoops, preceding a second set of tests studying the effect of different spacing between hoops of known dimension and in what pattern they are

arranged on the object. As with draft angle, the nature of free path texture is dependent on the solidifying behavior of the current glass formulation, and a quicker or slower setting glass chemistry would alter that design space accordingly.

List of Experiments and Results: Free Path

Free Path Printing			
object #	R min [mm]	R max [mm]	pattern
1	1	6	linear
2	10	20	linear
3	10	20	linear +300% feed rate
4	10	20	helical
5	10	10	bifurcating
6	11	11	bifurcating
7	12	12	bifurcating
8	14	14	bifurcating

Table 3.5: list of free path printing experiments

Hoops ranging from 5 mm radius to 20 mm radius were tested with 5 standard layers between sets in order to record their effect on printing as isolated features, and all produced stable print conditions, along with a range of visual distortions. Tests on hoop spacing provided a completely new surface finish to printed glass, no less stable for hoops as large as radius 11 mm. A test of 14 mm hoops, altered the layer deposition enough to destabilize the process, resulting in significant irregularities by the top of the object (figure 3-17).

Results of the free path printing experiments highlight the agency of molten glass in emergent design properties, and the need for material sensitivity in that design. The fabrication products are far from the CAD design input, but repeatable and optically distinct. A software heavy platform might find ways of predicting a single, theoretically exact geometry for the overhanging features, but would require very precise information in glass temperature, build chamber temperature, and adhesion characteristics of the material. To predict the optical distortion properties would require both the exact geometric form as well as the surface finish and refractive index of the glass at high precision. Instead, these features remain generated in a representative fashion using planar features, but understanding the constraints of

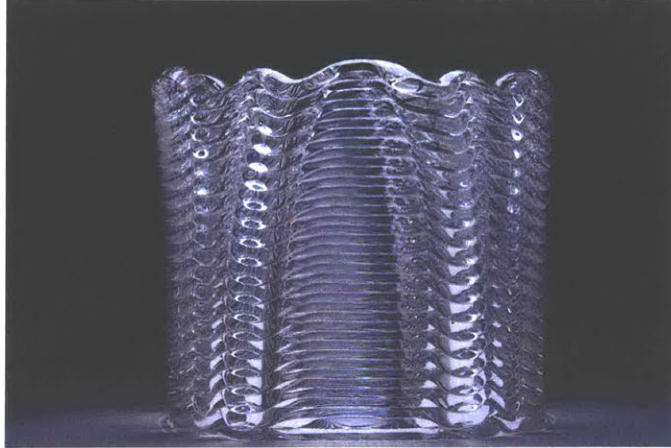


Figure 3-17: radius 14 mm hoop free path printing experiment with visible errors in planarity

the three dimensional products through a holistic, iterative testing approach allows the features to be used freely and remain emergent in specific form.

3.2.5 Conclusion of Forward Development

To conclude, a variety of different geometric and dimensional process parameters in glass 3D printing were explored, including feed rate, layer height, draft angle and *free path* printing, and an established range of possible parameters and limits were defined for each printing condition, including integrating multiple conditions in a single test. These conditions are commonly understood for most additive manufacturing platforms. For an off the shelf plastic printer, this is a simple exercise in fine tuning of settings, often accomplished within a single benchmark object which can incorporate as many different conditions as possible for the most efficient machine calibration possible. The National Institute of Standards and Technology (NIST) reports a standard test part [15] that exhibits a large range of feature sizes, overhang angles, enclosed volumes, and support material structures. On the other hand, the relative instability of molten glass deposition and large feature size create a scenario with relatively few addressable voxels available per object, given the build volume and a more sensitive approach is required. Indeed we see examples like in section 3.2.4 where one parameter, in this case layer height, affects or even enables another, in this case draft angle.

Given the potential diversity of designs with an AM system, exact tests of every possible geometry and combination of print conditions is of infeasible scope. Instead, the generation of material sensitive test object designs, able to explore ranges of different parameters at once and account for the variability of the machine, is key to building a design space not from discrete points, but of established design vectors. In the next sections, we will take this a step further, examining forms which result from material interactions completely beyond the design input space, which operate at sub-filament scale and generate even more complex physical and optical forms.

3.3 Sub-filament Scale Fabrication

While the G3DP2 system is reliant on dynamic material interaction to describe the exact geometric forms produced, as shown in the previous sections, some specific material behaviors not only dictate the geometry but create entirely new hierarchies of structures. In some cases, the behavior of viscous, molten glass generates filament geometries at smaller scales than filaments themselves resulting in deposition paths far more complex and at finer resolution than the designed tool paths. These are exemplary of a design hierarchy that takes advantage of the material behavior to generate functionality across multiple scales while only designing at a single scale. In the glass printing process, both a self coiling and horizontal fiber drawing behavior have been observed.

3.3.1 Autocoiling Phenomenon

Well known in the field of fluid dynamics, viscoelastic liquids, especially those of high viscosity exhibit a self coiling behavior. Termed *autocoiling*, the phenomenon is observed when fluid is extruded at a high offset between nozzle and substrate such that it acts a thin cylindrical rod and buckles under self-loading. The buckling instability is similar to classical Euler buckling, but the continuous flow of material results in a dynamic instability, and metastable coiling behavior which can go on indefinitely as long as the viscosity, offset, and pressure remain the same. Mathematicians specializing in fluid dynamics study this phenomenon in high viscosity oils and in everyday life, one might observe it while drizzling honey or syrup over a starchy breakfast, but the nature of molten glass fabrication is to solidify geometries created by viscosity and elasticity dynamics, so autocoiling can be a way of fabricating highly complex curved and looping structures.

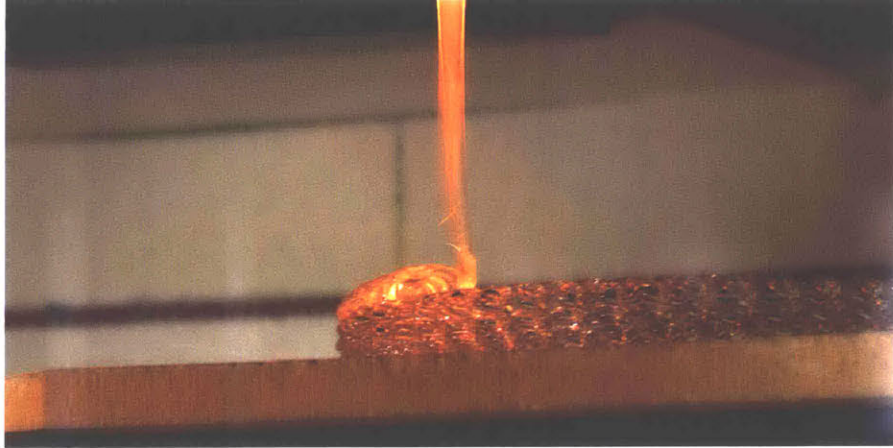


Figure 3-18: autocoiling of molten glass at extrusion offset 100mm

Detailed in the research article *The Molten Glass Sewing Machine*, the G3DP project explored the possibility of autocoiled fabrication utilizing the CNC control system of the glass printer [31]. Fluid dynamics research by Pierre Brun of the MIT Department of Mathematics reveals a powerful tool for simulation of the 3D viscous coiling process enabling the designers to predict the exact forms generate in glass and then control their deposition using precision machine control of glass temperature, nozzle offset, and travel speeds, the coiling parameters (figure 3-19).

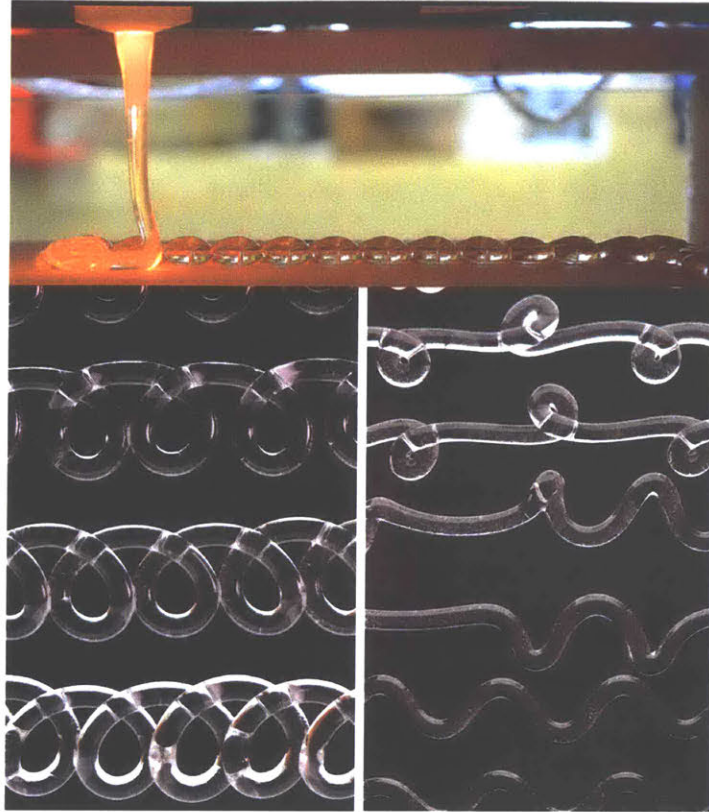


Figure 3-19: The molten glass sewing machine. (top) The nozzle is advected horizontally. (left) translated coils and (right) alternated loops and meanders
image and caption credit : P.-T. Brun [31]

The structures created through this process have much tighter available curvature, overlapping filaments and thinner filaments compared to those generated by normal printing conditions, and are tunable using the parameters described in figure 3-19. Stacking layers of coiled structures can be accomplished by offsetting standard printing tool paths by $100mm$ in order to initiate the desired coiling behavior (figure 3-18).

Autocoiled Products

In order to leverage the coiling behavior of glass into the product scale design space, a series of experimental objects were printed to test the transitions between normal printing and autocoiling. The first transition, switching from 5mm nozzle offset to 100mm offset, was explored for the first time. After printing 20 layers of standard 5mm layers, the nozzle offset is increased with a (z) axis feed rate of 100mm/s (compared to the 10mm/s feed rate in (x, y)). The high rate of change is chosen to minimize the transitional print condition which is observed to be less consistent than either standard printing or autocoiling. The result of this transition can be observed as aberrant filament deposition in the object shown in figure 3-20.

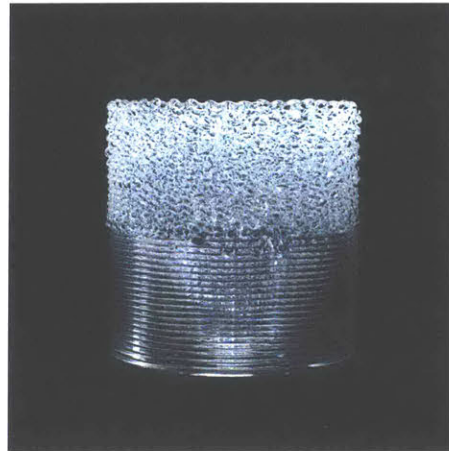


Figure 3-20: autocoiled object with unpredictable loops at the point of transition (center of object)

3.3.2 Bridging

The second sub-filament scale behavior observed in glass printing was a fluid flow instability which lacks a complete understanding at the time of writing. It has been observed as a failure mode in some printed objects seemingly as a result of underadhesion and asymmetric shear forces between printed layers. The symptoms are an underextrusion and separation between the current printed layer and previously printed layer. The nozzle continues to move along the tool path, but without the adhesion to the layer below, draws a thin fiber that remains self supporting and cools without joining the layers below it. Eventually, pressure in the nozzle causes the extrusion to reattach, resulting in free-floating glass "bridge" (figure 3-21).

While autocoiling glass can be related to other viscous fluid instability and even more generally to a classic thin member buckling problem, this dynamic adhesion problem presents with a number of key thermodynamic

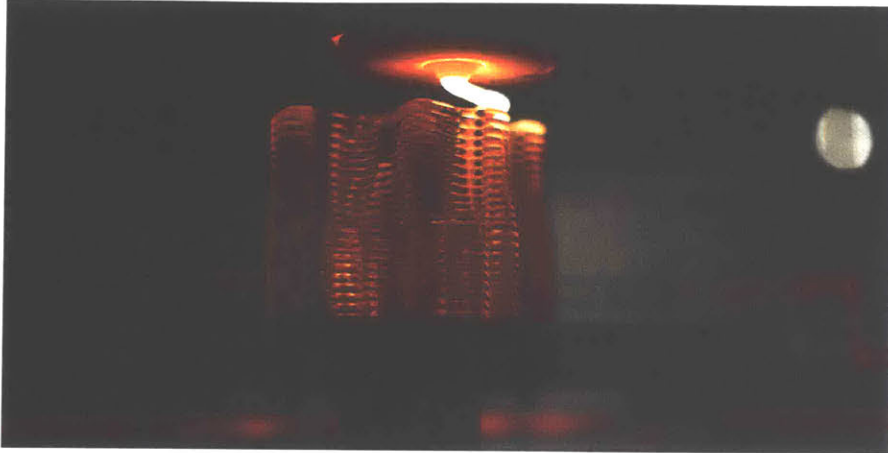


Figure 3-21: bridging phenomenon during printing; experimental settings to facilitate the process included high print speeds and sharp corner

parameters that remain prohibitive to measure without disturbing the flow itself (i.e. with a thermocouple physically in contact with the glass). Any computational models of the process require adhesion properties of both glass layers, as well as the cooling and solidifying behavior of the extruded glass, all of which are heavily temperature dependent. For this reason, it is not fully understood what causes the instability to manifest⁷, but when it does it enters a clear regime of complex structures superimposed over the tool path geometry. An emergent behavior, it could provide the glass printing designer with access to much finer scale material behavior by altering those thermodynamic properties to initiate bridging. An example of such emergent control is shown in figure 3-22 where two identical tool paths are used to generate entirely different geometric forms.

⁷A promising parallel research avenue is in using high resolution infrared thermography to measure temperature of all bodies during the process, but highly reflective and low emissivity materials like molten glass are extremely difficult to measure accurately. Still, a thermal imaging system if calibrated, could read temperatures without disturbing flow and that data might be used in combination with computational fluid models simulating the behavior



Figure 3-22: (a) cylindrical tool path under standard print conditions and (b) identical tool path showing adhesion errors and bridging instability phenomenon

3.3.3 Towards a New Product Space

The ability to harness glass instabilities as design tools is still early in its development. Early experiments in using auto-coiled glass in concert with printed glass show promising results, and bridging phenomena are not so understood but increasingly well documented for further research. Print conditions at filament scale and greater, however, are coming to fruition as a full pallet of design vectors for glass printing. As detailed in this chapter, a catalogue of test designs and potential product scale forms have been generated leading to the capacity for functional products. The next and final chapter of this thesis explores one of these new functional spaces as we look towards the architectural scale production of glass. A set of vascular products is generated, pulling from the experiments and results of this design space analysis.

Chapter 4

Conclusion: Towards Vascular Architecture

4.1 3D Printed Vessels

The concept of a vessel made from glass is nearly as old as the material itself. Even before the invention of blown glass, vessels were made by core forming, a process involving casting glassy materials around a removable internal mold [11]. In contemporary scientific practice, the chemical inertness and chemical resistance of glass make it ideal for containing chemical and biological systems at work, and of course observing them through an optically clear substrate. Glass is preferred here to even the strongest polymer vessels. As these are properties intrinsic to the material, we experiment with the possibilities of complex vessels generated by 3D printed glass and their potential applications.

It cannot be assumed that additive manufacturing tools generate components which are air or water tight. For example, injection molded PLA plastic might be watertight under correct process conditions, largely thanks to high pressure creating dense parts, but the process conditions for 3D printing with the same material typically yield high porosity, and poor sealing between layers and filament paths [27]. For printed glass, however, we observe complete adhesion between layers and no porosity in the material, making it a suitable process for producing vessel walls.

Up to this point, all of the objects produced by G3DP and G3DP2 had been single walled structures, unsealed at the top and bottom. The flow characteristics of glass during the printing process can be highly sensitive

to disturbances, and crossing over or overlapping with previously extruded, solid glass filaments is a risk both to the fidelity of the desired output, and to the safety of the machine. Delicate ceramic machine components can be easily damaged by crashing the nozzle into newly solid glass objects. The output of glass printers then is largely characterized by a cylindrical topology, with much variety in geometric form and design. Capping either end of these cylinders is straightforward; the wall faces on top or bottom can be sawed, ground, and polished into perfectly level surfaces, and joined to standard plate glass with silicone or epoxy resins to create a single or doubly capped vessel.



Figure 4-1: 3D printed glass vessel, with colored liquid illustrating multiple channels

Still, the distinct advantage of the additive manufacturing platform is surely in its ability to generate complex and unique geometry and while this can be applied to single walled, single channel, systems, being able to shift morphology into multiple channels or even continuously changing morphology between one or more channels would offer dramatically richer application and design space for large scale glass fluidics including mixing or separating any number of liquids, gases, or even biological media. To achieve this, the team developed a design system for bringing together sections of glass filaments which lie on the same layer, sealing off sections of the internal channel, thus creating multiple channels. Doing so required an understanding of the

glass deposition and the potential risks to printed object and to the printer itself and system for custom machine tool paths capable of managing those limitations.

4.1.1 Bilobe Design and First Principles of Multi-Channel Glass

With most conventional plastic FDM 3D printers, there is little risk in crossing or merging filaments on the same layer, as there is often flexibility in the machine itself, and in the flow characteristics of the material. Many systems also use start and stop control to avoid generating errors in complex, interconnected tool paths. Without such control available, and with sensitive deposition characteristics, in order to begin connecting paths and producing channels in glass printing, limitations on when and how paths might connect need to be carefully considered and designed for.

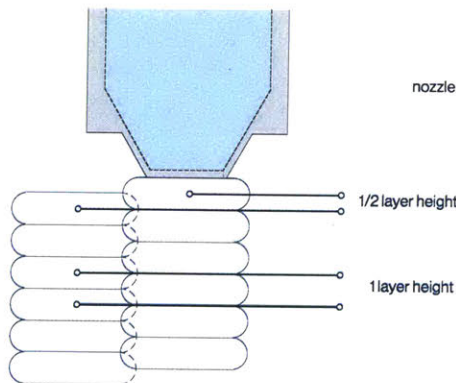


Figure 4-2: diagram of overlapping glass printed layers showing half layer step offset and nozzle clearance

layer stack could provide horizontal overlap without the nozzle tip coming too close to the solid glass in previous part of the layer. Path planning for layers to fold in on themselves and overlap at exactly a one half layer would require coordinated z-height along a given layer, which we refer to as *active z printing*.

The first example of this method takes advantage of a unique case in path length symmetry. To print without start and stop control, a continuous tool

The major risk in connecting paths is the rigidity of both the previously deposited filament and the ceramic nozzle. At less than a millimeter thick in the wall of the nozzle tip, even a small impact with solid glass causes irreparable damage the orifice, resulting in print failure. As a method of mitigating this failure mode, it was considered that overlapping filaments—that is to say filaments whose centerlines are less than one filament width apart—might be safely achieved if they were connected one half layer height (in the Z direction) apart. As shown in figure 4-2, this interlocking

path is used creating interpolated helices with continuous z-axis velocity unlike conventional tool paths where separate planar curves are generated layer by layer.¹ This means that for an arbitrary layer, any two points separated by half a layer length are also one half the layer height (which is also the pitch of the helix) apart. For example, with a circular helix, any two points on opposite sides of the circle are exactly a half layer step apart, and this applies to any arbitrary curve so long as the points are at the furthest point away from each other along that curve. So, without actively altering the pitch of a helical tool path, there will always exist two points per layer that may be joined at this optimal half layer step apart. This first experimental multichannel printed object was designed to make use of that symmetry condition by joining the opposite points of a 300 mm diameter circle at the center. The result is two 50 mm radius lobes (in plan) which were sealed off from each other. This part is designated a *bi-lobe* for this reason. In order to ensure that the lobes would seal, the joined section was extended a line, length 60 mm, instead of a single contact point along the curve. While only the exact center point exhibits this interlocking layer characteristic, by extending the region to a line, we hoped to account for any irregularity or hysteresis that might cause the test to give a false negative.

¹Flow control for G3DP/G3DP2 is, again, gravity-fed, and adjusted by temperature and material viscosity. To stop the flow of glass would require a change in gravity (pressure) or viscosity (temperature). The latter is available, but slow to respond

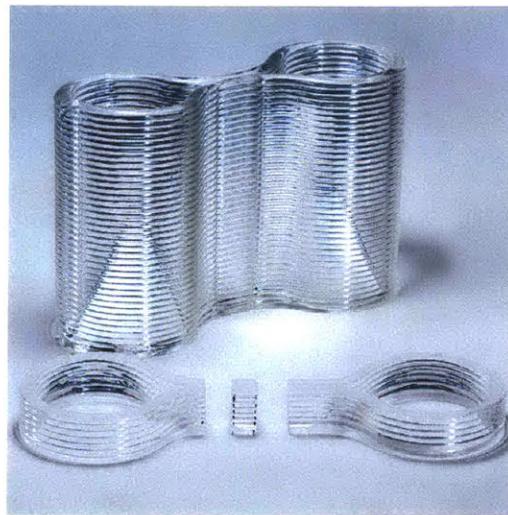
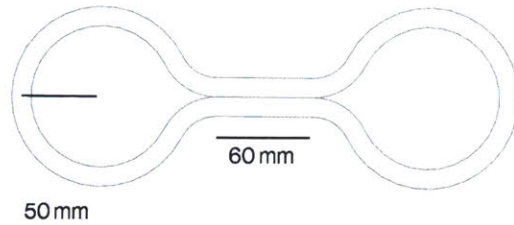


Figure 4-3: (top) diagram and dimensions of the bilobe form and (bottom) object printed in glass with sawed and sectioned samples

The resulting object was post-processed to keep a flat surface on its bottom face, then fixed to a piece of plate glass and sealed to it with silicone, which was allowed to cure for a recommended twenty four hours. Once the sealant cured, the two lobes were filled with red and blue dyed liquid and left to observe whether or not the channels were completely sealed off from each other. The bilobe was left for over 168 hours (one week) without any change (figure 4-1). After this test, part of the object was sawed off and then again along the center of the joined region for sectional analysis.

4.1.2 Active Z Toolpathing

The bilobe is a case in symmetry which only occurs at this specific nexus point. It is a two-fold symmetry that only allows for no more than two channels which must be of equal perimeter. Making multiple folds would not satisfy the condition of connecting filaments at a half layer height apart. Within these constraints is diverse design space of channel morphology, but as with single channel morphology, we are interested in expanding not just the geometric design space but the topological design space as well. A digital design tool is required to explicitly control the Z-axis travel.

Here, *active z* toolpathing method is described as generating a path by dividing the functionality of path segments into one of two categories:

1. joined segments — sections of layers that overlap in (x, y) plane to seal between channels
2. driving segments — sections of layers which do not overlap, and during which z height change is accommodated

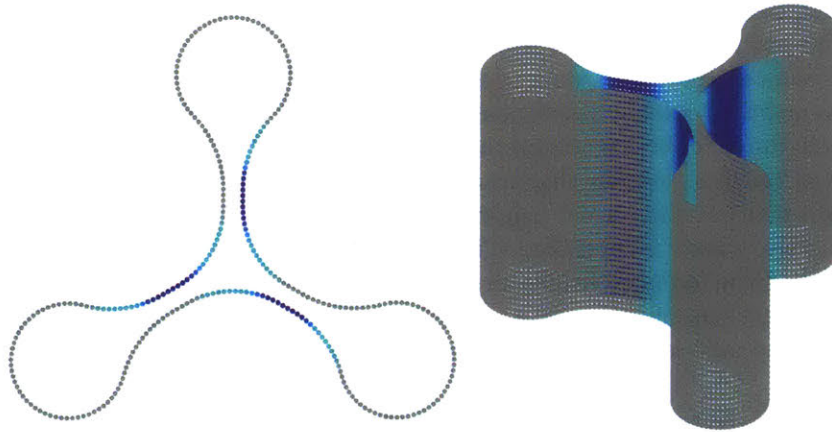


Figure 4-4: visualization of active-z toolpathing. Grey segments of the tool path represent flat sections which are joined with the driving segments shown in a cyan-blue gradient from least to greatest relative z-height. The path is sloped upwards (cyan) to meet the earlier flat section (grey) one half layer above it, fusing along the length in blue, and then sloped back down (cyan) to the previous layerheight.

Standard G3DP and G3DP2 tool paths are continuous helices, but in order to control the (z) axis position of filaments to accomplish appropriate layer stacking and overlap, the helix pitch is flattened in sections which need to overlap at specific heights, and the pitch is increased or decreased between those sections so that over the course of a single layer, one full layer step is still achieved. An initial experiment built on the the same geometric language at the bilobe, but without the two-fold symmetry condition. A 300 mm diameter circle, folded into three lobes (and so designated *trilobe*) with three overlapping points was designed with the active- z method.

The path travels in the negative (z) direction before the connection points and then quickly travels positively in the (z) direction around the lobes in order to overlap that connection point at the correct height.

Each active z layer is concluded with an increase in height so that each layer gains the intended layer height on every pass. Figure 4-4 shows a visualization of slope continuously along the path, and reveals the actual position as it moves up and down in order to overlap at the correct height.

4.1.3 Further Experiments and Potential Applications

So far we have shown functional fluidic or vessel prototype objects at three levels. The first is single channel vessels, the second symmetry-enabled double channeled vessels, and the third non-symmetric, actively constrained multi- or modular channel vessels. They stand as a proof of concept for multi-walled structures in 3D printed glass and from there, the team has outlined a set of experiments.

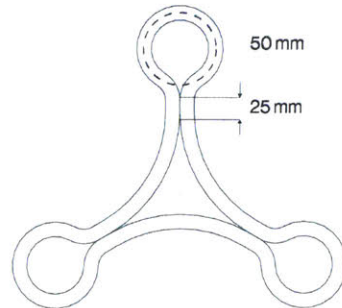
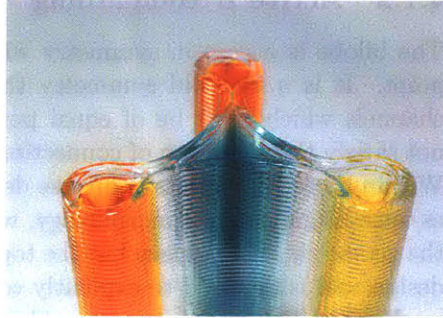


Figure 4-5: (top) glass printed trilobe object filled with fluid illustrating the four available channels and (bottom) plan diagram with channel radius and fused length dimensions

Channel Formation Parameters

After proof of concept, a set of design experiments was developed to test the parameters of glass filament overlapping and by extension, formation of sealed channels.

The most straightforward parameter to study is the *overlap spacing*, the amount of glass from a single filament that lies in the same (x, y) space as the filaments above and below it. The first experiments, the bilobe and trilobe, assumed an overlap of 6 mm (50% of layer width), which was an assumption made to ensure that, should the concept be sound, it would have the greatest probability of creating a seal between lobes. In order to test the required overlap spacing, different bilobe designs were generated with varying spacing in the overlapping section.

Slightly more subtle than overlap spacing is the length of filament which is overlapping, or the *overlap length*. Analyzing the cross section of these overlapping designs, it might appear binary, whether or not the spacing between layers is filled causing channels or lobes to seal apart from each other. However, the high viscosity of the molten glass often leads to slow response to changes in flow or print characteristics. A kind of hysteresis is observed in this layer overlap design, as well as other non-uniform printing methods, which means that a single point will not necessarily generate the desired printing condition, in this case, fully fused filaments. Only if the characteristic print condition is maintained for a period will it reach a steady state, and that delay in change is likely unique to each print condition as it will depend on the composition of all viscoelastic motion and forces present in the system. As with overlap spacing, a number of bilobe geometries (table 4.1) were designed with varying overlap length, from single point overlap to 100mm.

fluidics : bilobe experiments			
object #	channel radius [mm]	overlap length [mm]	overlap spacing [%]
1	50	60	50
2	50	5	50
3	50	0*	50
4	50	60	25

Table 4.1: list of fluidic experiments in radius 50 mm channel bilobe geometry with varying fused length and overlap spacing (*, single point fused distance)

Channel Morphology and Future Design

The next set of experiments with closed channels generated dynamic topologies. Using the active-z proof of concept, and the parameters understood from experiments with overlap spacing and length, a set of objects was generated with continuously morphing channel topology. Rather than linear extrusions, the design of these morphing channels changes from a cylinder to two channels and then to four channels. Given the maximum print height of G3DP2, the full morphing structure was divided into four sections, each 200mm in height. These sections were then post-processed, sawed, ground and polished to flat, level surfaces and designed to be sealed to each other using clear epoxy adhesive (HXTAL NYL-1).

This final construct brings together an empirical understanding of many interactions in the glass printing process. From glass filament dimensional parameters and accuracy, to active-z custom toolpathing, and layer to layer adhesion interactions. All of these interactions have been observed to result in catastrophic failure of printing and critical damage to the machine, so a sensitivity to material interaction, gained by extensive and iterative parametric testing, is key to the ability to produce such complex and dynamic structures.

Fluidics, or other forms of volumetric pathways, have a well defined place in the glass industry as well as research in chemistry, biology, and medicine. The volumetric scale of printed glass—and printed glass fluidics—has been more appropriate for applications as large in scale as architecture, including its installation at that scale. The ability to produce static or dynamic vasculature at the architectural scale may well leverage the performance and flexibility of the G3DP2 platform to generate new design applications. A column, wall, or facade of morphing fluid filled vasculature can tune its ability to store thermal energy, or tune its opacity at the resolution of a single layer by increasing radius or channels or splitting into any number of discrete sections. If actual fluid or gas flow is incorporated into these structures, it opens up the possibility for turbulent mixing of different compounds in order to accomplish thermo-chemical tasks. Examples of experimental architecture using bacterial factories as bioreactors generate energy through vasculature and mixing of nutrients while removing waste [14]. 3D printed glass vasculature might provide easily customizable vascular architectures created out of the ideal material for containing biological systems like these.

Future research and development of these systems should involve a thermal characterization of fluid or gas filled glass volumes in order to understand

the capabilities of a system that represents a continuously tunable version of many building envelope insulation systems which use different materials in discreet volumes. Pursuing this direction would entail the exploration of plumbing and flow in printed glass, testing the requirements and consequences of dynamic fluids rather than static volumes.



Figure 4-6: 4 component fluidic structure with morphing sectional topology with sections at joints and ends shown right 75

4.2 Vascular Architecture in the Future

While the design space for vascular architectural scale components in printed glass is barely in its infancy, preliminary models for performance are beginning to come together in parallel. Based on what kinds of forms seem to be feasible in glass fluidics, two potential performance modeling systems were explored to evaluate the thermal and optical performance of printed glass. In applications of this scale, the relative performance metrics relate specifically to building energy systems including HVAC and daylighting and there are any number of commercially available computational analysis suites for modeling these systems on top of existing CAD models of building systems and using traditional building materials². When a new system typology is introduced, those analyses must be addressed in a new way or else rebuilt from the ground up in order to accurately model their energy performance, and only by comparing those models to experimental data (and to potentially new system specific models) can we understand how such new systems perform. In this section I outline a brief example of analyzing new glass printed products with existing thermal modeling platforms, and alternately, an experimental set up and preliminary results for optical performance of glass printed products. The first exemplifies a performance space where the G3DP2 product output should fit into standard models and the later an example of a completely new performance output which does not and therefore needs new data and a new model to evaluate performance.

4.2.1 Preliminary Environmental Models

At a high level, the thermal performance of a building is evaluated by the energy required to heat, cool, and ventilate the entire system, given the site environment, so that the interior of the space is comfortable for its occupants. That evaluation can be subjective in that the true energy use of a building is dependent not just on its design but also its use and the behavior of the occupants. For example, a building might significantly drop its energy use if occupancy is commercial rather than residential, with less time spent conditioning the space, or even by occupants adjusting their preferences to cooler indoor temperatures in the winter and warmer temperatures in the

²examples include DIVA (Solemma LLC) for environmental modeling, Ladybug and Honeybee (Ladybug Tools LLC) for daylighting analysis, and Energy (US Department of Energy) for comprehensive building energy analysis

summer ³. In short, the thermal performance of a building is more than just a sum of its materials' properties. Nevertheless, every building material used has its own set of thermal performance properties this is where we begin for printed glass components as well. Whether competitive or not compared to traditional building materials will have some relevance not necessarily on *if* it makes sense as a contemporary building material but instead on *how* it might be used as a future building material.

U-Value

Thermal performance of a material is measured by its resistance to thermal change. Regardless of the temperature of the external environment, it costs no energy to maintain a comfortable temperature if the building envelope does not transmit energy (heat) either from the inside to outside or outside to inside. For this reason, good insulating materials, which have high thermal resistance, are desirable for low energy buildings. Quantitatively, thermal resistance is described as the thickness divided by the thermal conductivity of all materials in the envelope. For a typical building envelope, this can be a composite of drywalling, concrete or masonry, wooden studs, and commercial insulation material. The resulting value, a measure of unit thickness per conductivity, is then inverted to provide a heat transfer coefficient, the U-Value for a material or composite (equation 4.1). The U-value is the measure of heat transfer per unit area, and the lower the value, the better the material is at insulating.

$$R = \frac{\text{material thickness [m]}}{\text{thermal conductivity [Watts/m}^\circ\text{K]}} \quad (4.1)$$

$$U = \frac{1}{R}$$

Glass Printing Model

The heat transfer coefficient was calculated for a hypothetical glass printed envelope by modeling the thickness and connectivity of a printable sample component. Using the established printed channel design space (section

³While general perception that about 22°C is the most agreeable indoor temperature, human comfort can actually be described as more of a moving target, with ideal temperatures relating more to the recent history of outdoor climate. This is known as the adaptive human comfort model [10]

4.1.1-4.1.3), a 3 channel component was described by width $300mm$, the widest build volume dimension of G3DP2, channel thickness $50mm$, and wall thickness $12mm$. The resulting component has total dimensions of $324mm * 198mm$. Finally, to simulate a modular component to cover any arbitrary area of envelope, a silicone joining layer $4mm$ in thickness was modeled between components. The resulting modular envelope is visualized in figure 4-7. In modeling composite materials, materials stacked between interior and exterior are additive in resistance while materials sharing in-plane thickness (stacked perpendicular to the inside to outside vector) average by the ratio of their thickness. A project by German environmental engineer Ralf Plag provides a free to use service in calculating U-value based on any number of materials with specified thickness and arrangement, which was used to calculate the U-value for our hypothetical glass printed envelope [47].

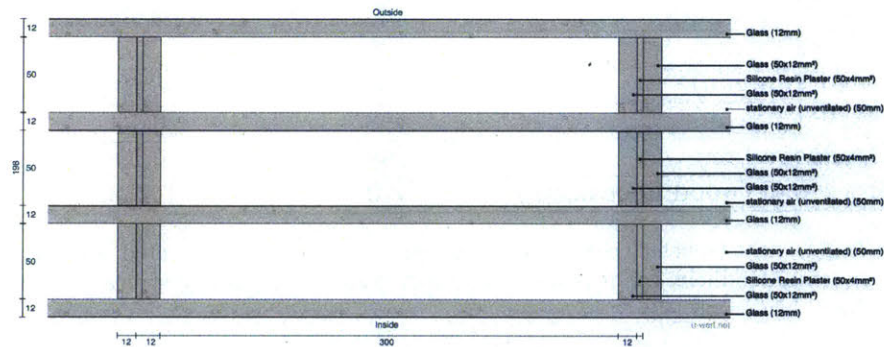


Figure 4-7: composite dimensional model of 3 channel glass printed building envelope generate using U-Value Calculator[47]

This model included sections of standing air within the channels as a baseline for a system we know to be fabricable with no further development of the G3DP2 system, and the complete U-value calculation presented a value of $2.60W/m^2 \circ K$. By comparison, commercially available, machine-blown glass channel facade systems offer a U-value range of $0.49 - 0.19W/m^2 \circ K$ (SF-60 Channel Glass, Bendheim Wall Systems [49]) or up to 92.7% better thermal resistance than the proposed model. Commercial systems like Bendheim's Channel Glass face the same difficulties in material properties, but to increase thermal resistance, thermal breaks are used at component seams to prevent heat transfer at the edges. Going even further, the air

inside the channels is often replaced with a lower thermal conductivity gas (such as argon or xenon) or else partially or fully evacuated so that it operates as vacuum insulation, one of the best insulating material available. Leveraging the power of additive manufacturing is to embrace the resolution of customizability per component, and so the focus of multi-channel printed glass is to use it as a dynamic system, both in geometry and potentially in fluidic composition as well. To this end, U-values for the glass printed model were calculate for air filled channels, water filled channels, argon filled channels and evacuated channels and reported along with the Bendheim facade systems and a model for a typical brick wall with external insulation (made from wood fiber) in table 4.2.

U-Value : G3DP2 vs contemporary building systems		
system (fill)	thickness [mm]	U-Value [$W/m^2\text{ }^\circ K$]
G3DP2 (air)	198	2.60
G3DP2 (water)	198	2.10
G3DP2 (argon)	198	0.49
G3DP2 (vacuum)	198	0.45
Bendheim (air)	102	0.19
Brick wall (wood fiber insul.)	440	0.233

Table 4.2: heat transfer coefficients (u-value) for multi-channel printed glass with varying fill, Bendheim commercial curtain wall glass tubing [49] and typical external insulated brick wall [47]

Critically, the glass printed products have not yet been functionalized to the point of dynamic fluids, but the preliminary calculation of thermal properties are encouraging in the ranges they afford. Should a low-vacuum or low conductivity gas filling prove feasible, the potential envelope would be competitive with commercially available curtain walls, but with extreme capabilities for complex or unique component geometry in industrial scale manufacturing. If a dynamic fluid can be realized, the system can be tunable, enabling a near doubling in heat transfer, depending on the needs of the system at a given time. These values are high level in their calculation, and exclude the exact mechanics of how printed glass is fitted as an envelope, but they give a sense of the range of thermal capability for potential systems.

4.2.2 Preliminary Performance Testing

While heat flux is a condition that is often measured over the meter scale for building envelopes, a material's behavior with respect to solar radiation can be much more difficult to quantify. Heat conduction is related to bodies and contact surfaces where one-dimensional temperature profiles can be calculated across one-dimensional gradients. Light transmittance, reflectance, and absorption are multi-dimensional properties related to the three-dimensional geometry as well as wavelength spectrum of the light in question and the optical material properties of all materials involved. Building energy system models can account for the optical properties of glazing by modeling both the accurate transmission, reflection, and absorption properties in a building's CAD model using three-dimensional domes as representative sky models. From the dome, a series of rays with given intensities are traced in 3D space as they collide with the building model, and 3D representations of the surrounding site. Each collision is mathematically modeled to determine how much of the radiation was transmitted, absorbed, or reflected and in what direction, which is then used to trace the ray to the next collision.

Each environmental simulation of this type requires accountable optical properties for each piece of geometry in the model, and runs through a set number of collisions. The process is very similar to a ray traced rendering, but instead of generating an image, it generates data about how much solar radiation is absorbed into a building envelope, the aggregate of which is defined as total *solar gain*. Because of the limited number of ray collisions per simulation, the simplification that envelopes have perfectly planar texture on materials, especially reflective ones is made. The distinct and complex surface texture and high light transmittance of 3D printed glass make it a poor candidate for such models. The extremely complex caustic patterns generated by interaction of light and printed glass are also difficult to model even with very dense ray-tracing rendering systems, indicating that the less dense energy modeling systems would fail to represent the true nature of the interaction. Figure 4-8 shows the discrepancy between a standard solar radiation model and the high spacial-resolution intensity of caustic patterns from printed glass.

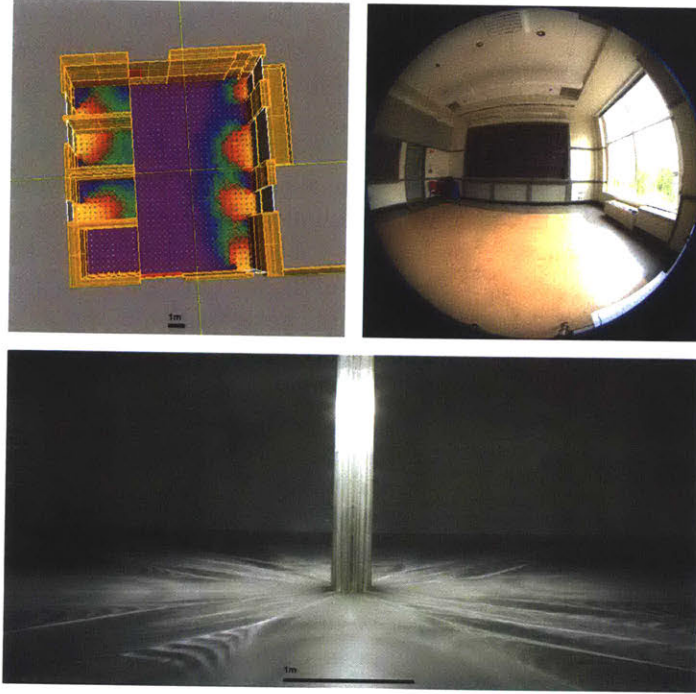


Figure 4-8: top perspective view of a typical light intensity map calculated by raytracing algorithms using DIVA environmental modeling platform and Rhino 3D CAD modeling platform (top left) and wide-angle view of the room being modeled (top right); by contrast, the much high resolution patterning of a printed glass column (bottom), which would be lost in the traditional modeling platform

Empirical Testing

Without a feasible route to modeling the complexity of printed glass geometry, a relative measurement experimental method was established to evaluate the optical behavior of printed glass objects. While the future of solar radiation modeling will require a new form of computational platform to model printed glass, in the meantime empirical testing can reveal trends and information about how the material interacts with light. Given that most of the experimental glass objects were printed as cylinders of varying print condition and surface texture, a light transmittance study was conducted by measuring the light intensity at the center of various cylindrical test prints under identical lighting conditions. Each cylinder was placed at the center of a seamless black backdrop and subjected to three distinct LED light panels. Measurements were taken using a light intensity meter (Extech Instruments) placed in the center of the object. An opaque baffle was used to cover the top of the cylinder so that all light recorded by the meter would have traveled through the glass itself. With three light sources, a total of seven permutations were available to measure per object (figure 4-9 shows a visualization of five permutations) and the light intensity for each is averaged for a given object. Using this method with objects of varying texture (as described in the Design Space section of this thesis), a small catalogue of relative light transmittance values were collected for different designs.

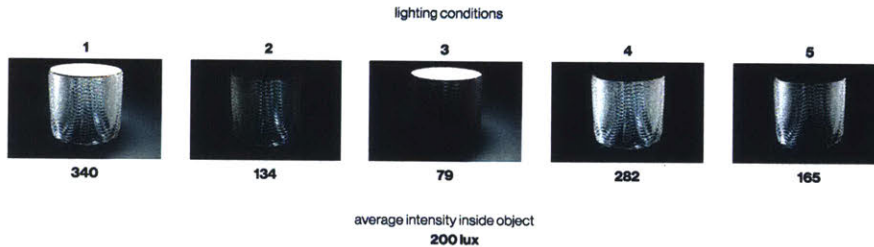


Figure 4-9: 5 distinct lighting conditions tested on a glass printed object with free path printing (section 3.2.4) surface texture; light intensity (measured in lux) at the center of the object is reported for each condition and averaged per object

Results

The most notable objects tested with the custom light transmittance experiment were a set of baseline normally printed cylinders, three cylinders printed using the autocoiling method (section 3.3.1) and three cylinders with free path "hoop" features (section 3.2.4). Their light transmittance data is reported in figure 4-10 by light intensity per object over three different lighting conditions (single light source, two light source, and three light source). Seven identical cylinders of standard condition printed glass were tested largely to verify that the relative lighting test would yield repeatable results across samples which should theoretically have the same surface texture and so should transmit roughly the same amount of light when placed in the same conditions. Indeed, all the cylinders fall around the same point, averaging a maximum light intensity of 202 lux (which was under the three-light condition). The two-light and single-light test followed a similar consistency.

The more textured objects, the autocoil and free path objects, were measured to have much higher light intensity inside, resulting seemingly from a much higher light transmittance given the conditions. One autocoiled object measured a maximum intensity of 405 lux and the free path objects a maximum intensity of 346 lux, an increase of 100% and 71% respectively compared to the baseline standard glass printed texture. This can be explained by the greater surface area of the more textured objects catching a greater number of incident light angles, reflecting and refracting light towards the inside of the object. As these textures are a result of print conditions now available as design vectors of the G3DP2 platform, they can be used to control the light transmittance of an object or architectural component at as fine a resolution as the textures can be printed. Further developing the design space of available print conditions and fine tuning the transitions between them also encourages the tunable interaction of solar energy and glass printed products.

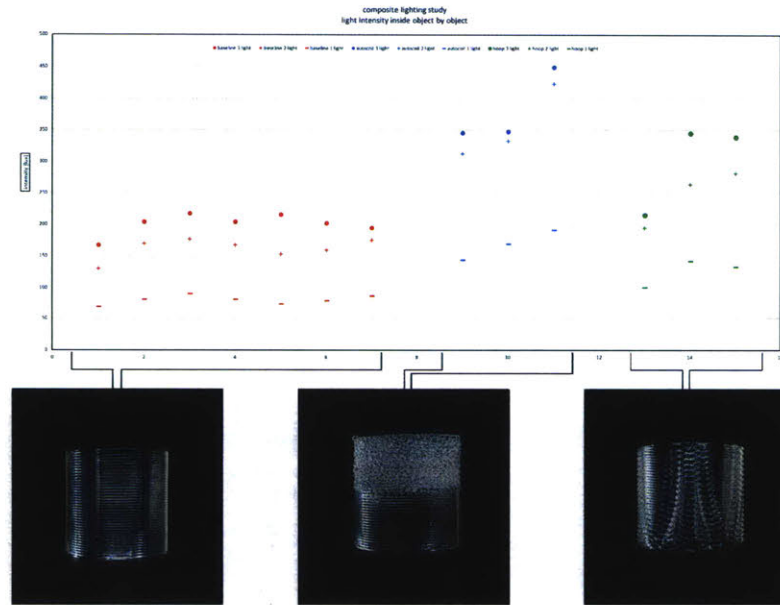


Figure 4-10: light intensity data collected from glass printed samples of different surface textures. Each print type is exemplified by the three photos underneath and colored data marker showing normal print condition (left, red), autocoiled glass (center, blue), and free path printing (right, green). Each object was subjected to 3 lighting conditions: three light sources (dot), two light sources (cross), and a single light source (dash).

4.3 Conclusion

3D printing of glass, as an industrial process, is gaining momentum and diversity of scope and scale. In the last three years alone, new projects have accomplished 3D printed glass at the 10^{-6} m scale using vat photopolymerization[36], the 10^{-3} m scale with bar stock fed material extrusion [29], and G3DP/G3DP2 using molten stock to fabricate at the $10^{0.5}$ meter scale by components. The application space for smaller scales has an immediately apparent breadth as a replacement for traditionally manufactured glass products. Chemically etched microfluidics might be replaced by a more flexible and potentially cheaper vat photopolymer printed alternative, and hand blown lab glass could be as well with filament based printing systems. Applications for glass in architecture, however, are largely limited planar environmental envelope systems made from float glass for the reason that large volumes of glass are difficult to manufacture at tolerances befitting its brittle failure modes. Exceptions include the static glass tube [49] and glass brick which remain mostly non-structural again due to the variability (and by extension, high cost for precision) in manufacturing of cast glass. A fully structural use even of simple rectangular bricks requires the degree of precision comparable to that of CNC digital fabrication tools [46]. Given that requirement, there should be rich design space for additive manufacturing of unique or customizable components which require that precision to construct with already [43]. There may be a shift from static glass bricks to dynamic ones, leveraging the flexibility of a 3D printing systems with the environmental mediation that glass already accomplishes for building systems. What the future holds for a glass ecology in architecture is impossible to quantify, but by applying novel glass printed designs to existing evaluation metrics as well as building new evaluation methods will be the process by which that new ecology is printed.

References

- [1] W. R. Merriam, “Twelfth census of the united states taken in the year 1900”, Tech. Rep., 1900.
- [2] E. Pratt, “The glass industry”, Department of Commerce, Tech. Rep., 1917.
- [3] R. Douglas and S. Frank, *A History of Glassmaking*. London and Tonbridge: The Whitefriars Press Ltd., 1972.
- [4] W. Vogel. Columbus, Ohio: American Ceramic Society, 1985, vol. 2.
- [5] K. Cascone, “The aesthetics of failure: “post-digital” tendencies in contemporary computer music”, *Computer Music Journal*, vol. 24, no. 4, pp. 12–18, 2000.
- [6] A. Fluegel, A. K. Arshneya, D. A. Earl, T. P. Seward, and D. Oksoy, “Improved composition-property relations in silicate glasses, part i: Viscosity”, *Proceedings of the 106th Annual Meeting of the American Ceramic Society, Ceramic Transactions*, vol. 170, pp. 129–143, 2004.
- [7] B. Addis, “The crystal palace and its place in structural history”, *International Journal of Space Structures*, vol. 21, no. 1, pp. 3–19, 2006.
- [8] NSG, “Pilkington and the flat glass industry”, Tech. Rep., 2010.
- [9] G. Marchelli, R. Prabhakar, D. Storti, and M. Ganter, “The guide to glass 3d printing: Developments, methods, diagnostics and results”, *Rapid Prototyping Journal*, vol. 17, no. 3, pp. 187–194, 2011.
- [10] M. K. Singh, S. Mahapatra, and S. Atreya, “Adaptive thermal comfort model for different climatic zones of north-east india”, *Applied Energy*, vol. 88, 2011.
- [11] K. B. Wight, *Molten Color : Glassmaking in Antiquity*. Los Angeles, California: J. Paul Getty Museum, 2011.

- [12] J. G. Fernandez and D. E. Ingber, “Unexpected strength and toughness in chitosan-fibroin laminates inspired by insect cuticle”, *Advanced Materials*, vol. 24, pp. 480–484, 2012.
- [13] P. Dilworth, M. Bogue, and D. Cowen, *3doodler 3d pen*, 2013.
- [14] C. I. GmbH, “Solarleaf bioraector facade”, Tech. Rep., 2013.
- [15] S. Moylan, J. Slotwinski, A. Cooke, K. Jurrens, and M. A. Donmez, “Proposal for a standardized test artifact for additive manufacturing machines and processes”, National Institute of Standards and Technology, Engineering Laboratory, Tech. Rep., 2013.
- [16] B. Glass. (2014). The vitrigraph kiln : Creating a new vocabulary in fused glass, [Online]. Available: https://www.bullseyeglass.com/images/stories/bullseye/PDF/TechNotes/technotes_02.pdf.
- [17] E. of Mathematics. (2014). Quadratic deviation, [Online]. Available: http://www.encyclopediaofmath.org/index.php?title=Quadratic_deviation&oldid=31480.
- [18] L. Mogas-Soldevilla, J. Duro-Royo, and N. Oxman, “Water-base robotic fabrication”, *Journal of 3D Printing and Additive Manufacturing*, vol. 1, no. 3, pp. 141–151, 2014.
- [19] N. B. S. .-. U. States, “Frequently asked questions about the national bim standard”, Tech. Rep., 2014, copied from archive.
- [20] S. Tibbits, “4d printing; multi-material shape change”, *Architectural Design*, vol. 84, pp. 116–121, 2014.
- [21] L. Wen, J. Weaver, and G. V. Lauder, “Biomimetic shark skin : Design, fabrication, and hydrodynamic function”, *The Journal of Experimental Biology*, vol. 217, pp. 1656–1666, 2014.
- [22] J. Duro-Royo, “Towards fabrication information modeling”, Master’s thesis, Massachusetts Institute of Technology, Program in Media Arts and Sciences, 2015.
- [23] J. Klein, M. Stern, M. Kayser, C. Inamura, G. Franchin, S. Dave, J. Weaver, P. Houk, P. Colombo, and N. Oxman, “Additive manufacturing of optically transparent glass”, *Journal of 3D Printing and Additive Manufacturing*, vol. 2, no. 3, pp. 92–105, 2015.
- [24] J. L. Lab. (2015). Mx3d bridge, [Online]. Available: <http://www.jorislaarman.com/work/mx3d-bridge/#top>.

- [25] L. Mogas-Soldevila, J. Duro-Royo, D. Lizardo, M. Kayser, W. Patrick, S. Sharma, S. Keating, J. Klein, C. Inamura, and N. Oxman, “Designing the ocean pavilion : Biomaterial templating of structural, manufacturing, and environmental performance”, 2015.
- [26] N. Oxman. (2015). Mediated matter : About, [Online]. Available: <http://matter.media.mit.edu/about>.
- [27] Stratasys. (2015). Sealing fdm parts, [Online]. Available: <http://www.stratasys.com/solutions/finishing-processes/sealing-fdm-parts>.
- [28] C. Bader, D. Kolb, J. C. Weaver, and N. Oxman, “Data-driven material modeling with functional advection for 3d printing of materially heterogeneous objects”, *3D Printing and Additive Manufacturing*, vol. 3, no. 2, pp. 71–78, 2016.
- [29] 3DPrinting. (2017). Micron3dp completes installation of pioneering glass 3d printer , prepares for beta release, [Online]. Available: <https://3dprint.com/167638/micron3dp-glass-3d-printer-beta/>.
- [30] Asiga. (2017). The pico 2, [Online]. Available: <https://www.asiga.com/products/printers/pico2/>.
- [31] P.-T. Brun, C. Inamura, M. Stern, G. Franchin, D. Lizardo, P. Houk, and N. Oxman, “The molten glass sewing machine”, *Philosophical Transactions A*, vol. 375, 2017.
- [32] D. Furnaces. (2017). Deltech positive pressure furnace used in fuel cell research, [Online]. Available: <http://www.deltechfurnaces.com/deltech-positive-pressure-furnaces-used-in-fuel-cell-research/>.
- [33] T. Gutowski, J. Sheng, D. Cooper, G. Corman, M. Hausmann, J. A. Manson, T. Schudeleit, K. Wegener, M. Sabelle, J. Ramos-Grez, and D. P. Sekulic, “Note on the rate and energy efficiency limits for additive manufacturing”, *Journal of Industrial Ecology*, vol. 21, S69–S79, 2017.
- [34] C. Inamura, “Towards a new metabolism: High fidelity additive manufacturing of functionally graded, optically transparent and spatially differentiated glass structures across scales”, Master of Science, Massachusetts Institute of Technology, Program in Media Arts and Sciences, 2017.

- [35] S. J. Keating, J. C. Leland, L. Cai, and N. Oxman, “Toward site-specific and self sufficient robotic fabrication on architectural scales”, *Science Robotics*, vol. 2, 2017.
- [36] F. Kotz, K. Arnold, W. Bauer, D. Schild, N. Keller, K. Sachsenheimer, T. M. Nargang, C. Richter, D. Helmer, and B. E. Rapp, “Three-dimensional printing of transparent fused silica glass”, *Nature*, vol. 544, no. 7650, pp. 337–339, 2017.
- [37] S. Manninger and M. del Campo, “Plato’s columns : Platonic geometries vs vague gestures in robotic construction”, 2017, pp. 374–381.
- [38] N. Oxman and The Mediated Matter Group, *Vespers: Lazarus*, The New Ancient Collection, London Design Museum, London GB, 2017.
- [39] T. Prototype. (2017). Micron3dp announces improved glass 3d printer, [Online]. Available: <http://www.Prototypetoday.Com/Micron3dp/Micron3dp-Announces-Improved-Glass-3d-Printer>.
- [40] R. Rael, V. S. Fratello, and P. Suon. (2017). Bad ombres v.2, [Online]. Available: <http://www.emergingobjects.com/project/bad-ombres-v-2/>.
- [41] A. Warburton. (2017). Goodbye uncanny valley, [Online]. Available: <http://alanwarburton.co.uk/goodbye-uncanny-valley/>.
- [42] T. Wohlers, “Wohlers report 2017. 3d printing and additive manufacturing state of the industry”, Tech. Rep., 2017.
- [43] C. Inamura, M. Stern, D. Lizardo, P. Houk, and N. Oxman, “High fidelity additive manufacturing of transparent glass structures”, under review, 2018.
- [44] —, “Industrial additive manufacturing of transparent glass structures”, *3DP+*, 2018, under review.
- [45] Lexus. (2018). Dazzling new lexus paint inspired by a butterfly, [Online]. Available: <https://www.lexus.com.au/about-lexus/news/dazzling-new-lexus-paint>.
- [46] F. Oikonomopoulou, T. Bristogianni, F. A. Veer, and R. Nijse, “The construction of the crystal houses façade: Challenges and innovations”, *Glass Structures & Engineering*, vol. 3, no. 1, pp. 87–108, 2018.
- [47] R. Plag. (2018). U-value calculator, [Online]. Available: <https://www.u-wert.net/u-wert-rechner/>.

- [48] statista. (2018). Glass industry, [Online]. Available: <https://www.statista.com/study/43866/glass-industry/>.
- [49] B. W. Systems, “Sf-60 channel glass frame system”, Tech. Rep., 2018.
- [50] Asiga. (). Precision on your desktop, [Online]. Available: https://www.asiga.com/media/main/files/printers/Pico%20Brochure_us_en.pdf.
- [51] U. Census. (). Age and sex 2007-2011 american community survey 5-year estimates, [Online]. Available: <https://www.census.gov>.
- [52] T. E. C. LLC, “The new standard for manufacturing from exon”, Tech. Rep.
- [53] T. B. Museum. (). Window pane, [Online]. Available: http://www.britishmuseum.org/research/collection_online/collection_object_details.aspx?objectId=466288&partId=1&searchText=roman>window&images=true&pa.
- [54] O. Uusitalo, “Springer briefs in applied sciences and technology float glass innovation in the flat glass industry”,
- [55] F. Wittel and T. Wagner. (). Science and engineering of glass and natural stone in construction, [Online]. Available: <http://www.ifb.ethz.ch/education/msc-courses/msc-science-of-glass-stone-in-construction.html>.